RESEARCH ARTICLE

Distinct allosteric remodeling of HIV-1 Env dynamics on virions by gp41-directed antibodies reveals two modes of neutralization

Wang Xu[1], Narendra Kumar Gonepudi[1], Junyu Liu[1], Yufan He[1], Revansiddha Katte[1], Ran Wang[2], Harry Baffour Awuah[1], Yang Han[1], Baoshan Zhang[3], Jian Yu[4], Bo Hu[2], David D Ho[4], Priyamvada Acharya[5,6,7], Peter D Kwong[3,4,8], Maolin Lu[1]*

[1]Department of Cellular and Molecular Biology, School of Medicine, The University of Texas at Tyler Health Science Center, Tyler, United States; [2]Department of Microbiology and Molecular Genetics, McGovern Medical School, University of Texas Health Science Center at Houston, Houston, United States; [3]Vaccine Research Center, National Institute of Allergy and Infectious Diseases, National Institutes of Health, Bethesda, United States; [4]Aaron Diamond AIDS Research Center, Department of Medicine, Vagelos College of Physicians and Surgeons, Columbia University, New York, United States; [5]Duke Human Vaccine Institute, Duke University, Durham, United States; [6]Department of Surgery, Duke University, Durham, United States; [7]Department of Biochemistry, Duke University, Durham, United States; [8]Department of Biochemistry and Molecular Biophysics, Columbia University, New York, United States

***For correspondence:** maolin.lu@uthct.edu

Competing interest: The authors declare that no competing interests exist.

Funding: See page 23

Preprint posted
28 January 2026
Sent for Review
16 February 2026
Reviewed preprint v1
17 April 2026
Reviewed preprint v2
11 September 2026
Version of Record
02 October 2026

Reviewing Editor: Volker Dötsch, Goethe University Frankfurt, Germany

This is an open-access article, free of all copyright, and may be freely reproduced, distributed, transmitted, modified, built upon, or otherwise used by anyone for any lawful purpose. The work is made available under the Creative Commons CC0 public domain dedication.

eLife Assessment

This manuscript reports an **important** study in which the authors apply smFRET imaging to probe HIV-1 Env conformational dynamics in the presence of antibodies. Previous implementations of smFRET imaging of HIV-1 Env, which focus on gp120 conformation, have yielded limited information on antibodies that target gp41. Through the cutting-edge application of smFRET imaging, the study provides **convincing** insights into the mechanisms of action of relevant antibodies.

Abstract HIV-1 envelope glycoprotein (Env), a gp120–gp41 trimer, undergoes coordinated conformational changes that drive membrane fusion and allow immune evasion by transiently concealing neutralization-sensitive epitopes. Most broadly neutralizing antibodies (bNAbs) target gp120, whereas a distinct subset recognizes conserved gp41 regions, such as the fusion peptide and the membrane-proximal external region; however, their impact on Env dynamics and associated neutralization mechanisms remains unclear. By using bioorthogonal tagging for single-molecule FRET, we monitored real-time bNAb-induced conformational sampling of Env on intact virions. Most gp41-directed bNAbs allosterically stabilized the prefusion-closed (PC) state, whereas the bivalent 10E8.4/iMab favored both PC and CD4-bound open (predominant) states. Antibodies redistributed the conformational populations of Env with modest kinetic effects, preserving a sequential transition pathway. These findings reveal two modes of neutralization for gp41-directed antibodies, fixing the PC conformation and opening it up – in both cases, with neutralization occurring via long-range allosteric control of Env dynamics.

Introduction

The HIV-1 envelope glycoprotein (Env) mediates the fusion of the viral and host cell membranes, enabling viral entry (**Wyatt and Sodroski, 1998**; **Chen, 2019**; **Wang et al., 2020**). As the sole viral protein coated on the virion surface, Env is a central focus for vaccine design and the development of therapeutic antibodies, small-molecule inhibitors, and fusion blockers (**Wang et al., 2020**; **Klasse et al., 2025**). Env assembles as a trimer of noncovalently associated gp120–gp41 heterodimers, with gp120 engaging the receptors CD4 and co-receptor (CCR5 or CXCR4) and gp41 driving membrane fusion (**Chen, 2019**; **Wang et al., 2020**; **Kwong et al., 1998**; **Pancera et al., 2014**; **Lyumkis et al., 2013**; **Shaik et al., 2019**). These Env trimers are present at low copy number (roughly 5–15 per virion), and although their exact stoichiometry remains unresolved, productive fusion may require the coordinated action of multiple trimers (**Yang et al., 2005**; **Yang et al., 2006**; **Sougrat et al., 2007**; **Liu et al., 2008**; **Klasse, 2007**; **Brandenberg et al., 2015a**; **Brandenberg et al., 2015b**; **Katte et al., 2025**). Env is highly dynamic, undergoing large conformational rearrangements (**Munro et al., 2014**; **Munro and Mothes, 2015**; **Herschhorn et al., 2016**; **Herschhorn et al., 2017**; **Ozorowski et al., 2017**; **Henderson et al., 2020**; **Alsahafi et al., 2019**). A key early step is the sequential opening of the three gp120 protomers, which swing outward to form a fully open, CD4-bound trimer that exposes the CD4- and co-receptor-binding sites and primes gp41 for fusion activation (**Ma et al., 2018**; **Dam et al., 2023**; **Li et al., 2023**). This is followed by transient intermediate states and the refolding of gp41 into a post-fusion conformation that leads to membrane fusion (**Chen, 2019**; **Wang et al., 2020**; **Lee et al., 2024**; **Thakur et al., 2025**; **Ladinsky et al., 2020**; **Buzon et al., 2010**; **Zhao et al., 2022**). This conformational plasticity, combined with a dense glycan shield and rapid sequence diversification, enables Env to evade immune pressure by transiently concealing or exposing neutralization-sensitive epitopes, known as 'conformational masking' (**Wang et al., 2020**; **Kwong et al., 2002**; **Haynes et al., 2019**). Despite these defenses, a distinct subset of antibodies, known as broadly neutralizing antibodies (bNAbs), can neutralize diverse HIV-1 isolates by targeting conserved sites of vulnerability across Env (**Klasse et al., 2025**; **Haynes et al., 2019**; **Sok and Burton, 2018**). These epitopes span multiple structural regions, including the V1V2 apex, V3 glycan supersite, CD4-binding site, gp120–gp41 interface, fusion peptide (FP), and the membrane-proximal external region (MPER) (**Klasse et al., 2025**; **Haynes et al., 2019**; **Sok and Burton, 2018**). Eliciting potent Env-directed bNAbs remains a central goal of HIV-1 vaccine development (**Klasse et al., 2025**; **Haynes et al., 2019**; **Sok and Burton, 2018**; **Haynes et al., 2023**; **Kwong and Mascola, 2018**). Understanding how Env dynamics, intrinsically linked to its fusogenic function, shapes bNAb-mediated neutralization is important for guiding antibody-based therapies and designing next-generation immunogens.

HIV-1 neutralization by bNAbs is multifaceted and likely involves overlapping mechanisms (**Klasse et al., 2025**; **Haynes et al., 2019**; **Ivan et al., 2019**). By exploiting structural and functional constraints on Env, bNAbs can neutralize Env by competing with receptor engagement, disrupting the conformational changes required for membrane fusion, penetrating into Env glycan holes, and/or trapping the trimer into specific states. Most current insights derive from static cryo-EM and crystal structures of soluble Env constructs (**Klasse et al., 2025**; **Haynes et al., 2023**; **Kwong and Mascola, 2018**), which capture discrete conformations with atomic details of molecular interactions but do not reveal the sequence, timing, or rates of transitions between states. For gp41 epitopes, specifically FP and MPER, which are recognized by some of the most potent bNAbs, it is unclear whether antibody binding exerts long-range allosteric effects on native Env dynamics, and the impact on the distribution and kinetics of conformational sampling along the gp120–gp41 axis remains poorly defined. Among those, the highly potent 10E8.4/iMab (**Huang et al., 2016**; **Padte et al., 2018**), which combines an MPER-directed arm with the CD4-targeting antibody Ibalizumab (iMab) and is currently in clinical trials, represents a particularly promising therapeutic strategy. However, neither structural nor dynamic analyses of its complex with Env have yet been performed, leaving unresolved both the Env conformations targeted by 10E8.4/iMab and its effects on Env dynamics.

Here, we address these knowledge gaps by combining site-specific bioorthogonal tagging (**Nikić et al., 2015**; **Sakin et al., 2017**; **Xu et al., 2025**) with single-molecule Förster Resonance Energy Transfer (smFRET) (**Roy et al., 2008**; **Juette et al., 2016**; **Lerner et al., 2018**; **Lu et al., 2019b**) to visualize the real-time conformational dynamics of full-length Env on intact virions. While prior work has analyzed gp120-directed antibodies using smFRET with fluorophores labeled on gp120 (**Munro et al., 2014**; **Lee et al., 2024**), gp41-directed antibodies have never been systematically investigated

by smFRET, in part due to the lack of a suitable FRET-pair labeling system. By using dual click labeling at gp120–gp41 positions, here we characterize the conformational ensemble of native Env and define how bNAbs targeting the gp120–gp41 interface, FP, and MPER allosterically remodel trimer dynamics. Our results reveal previously unobserved shifts in Env conformational sampling and two dynamic modes of neutralization, accompanied by modest changes in transition kinetics that preserve the intrinsic opening pathway. These findings provide a unique perspective on how gp41-directed bNAbs alter Env conformational dynamics through long-range allosteric effects, offering mechanistic insight into HIV-1 neutralization and informing strategies to exploit these vulnerabilities for vaccine and therapeutics development.

Results

Dual amber-click labeling and functional validation of Env trimers for smFRET

To investigate the conformational dynamics of full-length Env on intact HIV-1 virions, we employed a minimally invasive amber-click labeling strategy that combines amber suppression with click chemistry for smFRET studies (***Figure 1—figure supplement 1***, ***Figure 1—figure supplement 2***). Our previously developed amber-free HIV-1 system eliminates background amber (TAG) stop codons, allowing efficient site-specific incorporation of unnatural amino acids (ncAAs) into the target HIV-1 protein of interest (***Xu et al., 2025***; ***Ao et al., 2024***). By using this platform, we introduced TAG codons at $S401^{TAG}$ in gp120 and $R542^{TAG}$ in gp41 of Env_{BG505} (a transmitted/founder primary isolate, ***Figure 1A***) on the HIV-1_{Q23} viral backbone (HIV-1_{Q23} Env_{BG505}). These tagging sites (***Figure 1—figure supplement 1***) were strategically selected along the gp120–gp41 axis based on available structural details (***Pancera et al., 2014***; ***Ozorowski et al., 2017***; ***Kwon et al., 2015***; ***Li et al., 2020***), allowing them to report on inter-subunit movements during conformational transitions. Through genetic code expansion with an orthogonal tRNA/tRNA synthetase pair ($tRNA^{Pyl}$/$NESPylRS^{AF}$) (***Sakin et al., 2017***; ***Nikić et al., 2016***), we then incorporated the ncAA trans-cyclooct-2-en-L-lysine (TCO*A) at these amber-tagged sites for fluorophore attachment (***Figure 1—figure supplement 2***; ***Ao et al., 2024***; ***Plass et al., 2011***; ***Plass et al., 2012***). Site-specific conjugation of LD555-TTZ (donor, LD555: Cy3 derivative; TTZ: tetrazine) and LD655-TTZ (acceptor, LD655: Cy5 derivative) fluorophores was further achieved by click chemistry via strain-promoted inverse electron-demand Diels–Alder cycloaddition (SPIEDAC, ***Figure 1—figure supplement 2***; ***Blackman et al., 2008***; ***Nikić and Lemke, 2015***).

Throughout this study, $S401^{TAG}$ $R542^{TAG}$ denotes the construct, $S401^{ncAA}$ $R542^{ncAA}$ denotes ncAA-incorporated but unlabeled virions, S401* R542* denotes their fluorescently labeled counterparts, and we refer to these sites as the gp120–gp41 (S401–R542) probe pair; the gp120 V1V4 (N136–S401) probe pair is used as a reference perspective.

To ensure that the tagged Env retained its functionality and was suitable for smFRET studies, we first validated dual-ncAA-incorporated Env ($S401^{ncAA}$ $R542^{ncAA}$) on intact virions as well as fluorescently labeled forms (S401* R542*). We obtained approximately 20% dual-amber suppression efficiency for HIV-1_{Q23} Env_{BG505} $S401^{TAG}$ $R542^{TAG}$, as determined by the relative infectivity of produced virions compared to wild-type (WT) Env (***Figure 1–figure supplement 3a***). Importantly, click-chemistry labeling did not further reduce infectivity, with labeled and unlabeled virions exhibiting comparable infectivity (***Figure 1—figure supplement 3b***), indicating that fluorescent labeling did not appreciably impair Env function.

The reduced infectivity relative to WT primarily reflects the inherent limitations of amber suppression in mammalian cells rather than loss of Env function, as discussed previously (***Xu et al., 2025***; ***Ao et al., 2024***; ***Gonepudi et al., 2026***; ***Xu et al., 2026***). Amber suppression must compete with endogenous translation termination, and unintended readthrough of endogenous or viral amber codons can interfere with protein expression and virus production. We minimized the latter by using an amber-free provirus (***Ao et al., 2024***). Dual-ncAA incorporation requires two successful suppression events within the same Env molecule, further reducing overall efficiency. Given these constraints, the ~20% dual-amber suppression efficiency achieved here is within the expected range and comparable to previous studies (***Sakin et al., 2017***; ***Ao et al., 2024***).

Immunoblotting of prepared virions that were harvested from transfected cell supernatants confirmed that both TAG sites were successfully suppressed, proteolytically processed, and

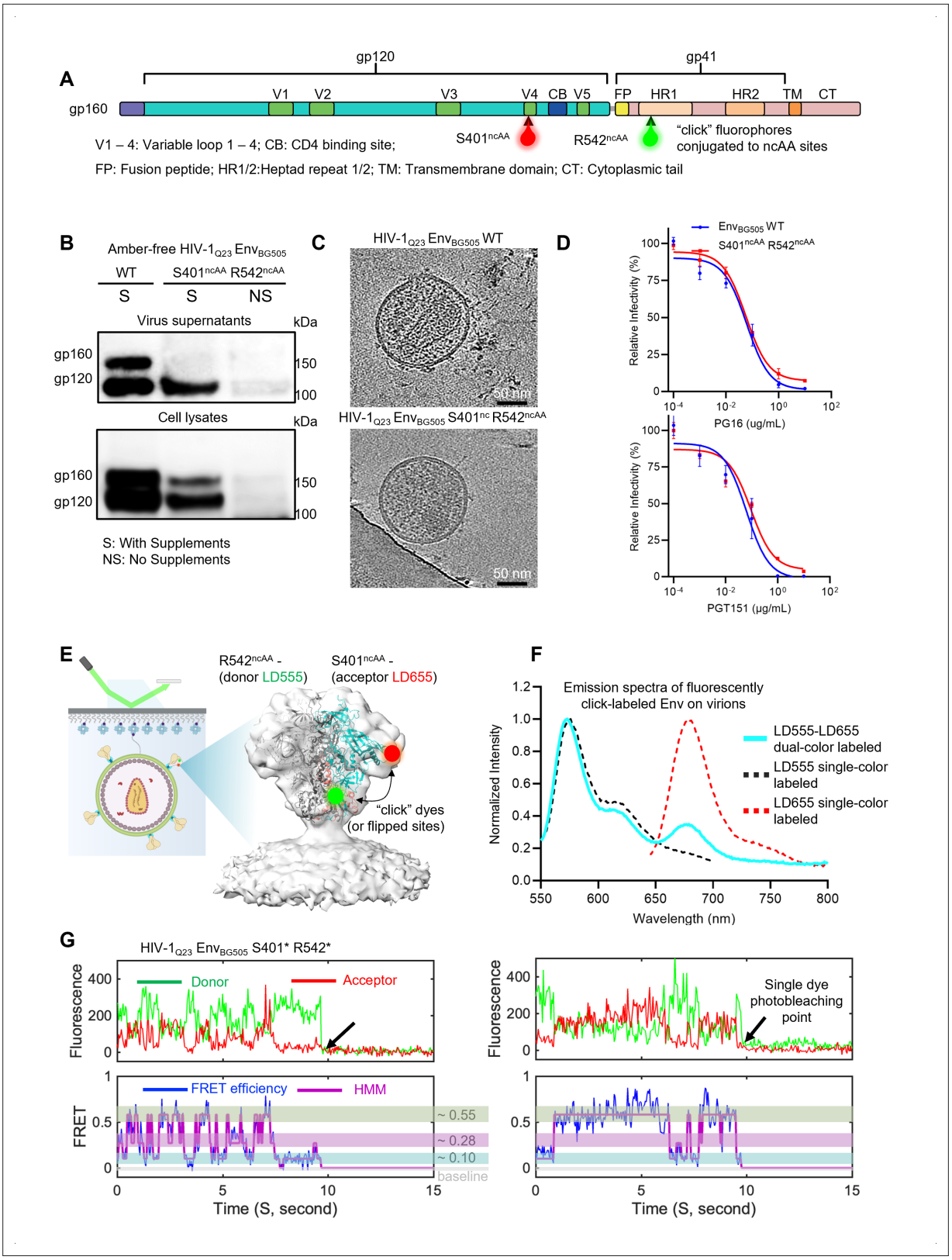


Figure 1. Single-molecule Förster Resonance Energy Transfer (smFRET) imaging of full-length Env on HIV-1 virions from the gp120–gp41 structural perspective. (**A**) Domain organization of BG505 Env with click fluorophores conjugated to ncAA sites at S401 on gp120 and R542 on gp41. 'ncAA' refers to unnatural amino acids incorporated at amber (TAG) sites via amber suppression, and 'click' dyes are site-specifically conjugated through click chemistry. (**B–D**) Functional validation of HIV-1_{Q23} Env_{BG505} $S401^{ncAA}$ $R542^{ncAA}$ virions for smFRET studies. Immunoblotting (**B**), tomographic slices (**C**), and

Figure 1 continued on next page

Figure 1 continued

neutralization curves (**D**, *n* = 4) confirm that the dual-ncAA incorporation does not compromise Env trimer functionality on virions used for smFRET. Viruses were generated by transfection with 100% of the indicated HIV-1 constructs, and the data shown represent the resulting particles. (**E**) HIV-1_{Q23} virions carrying fluorescently labeled full-length Env_{BG505}, imaged by prism-based TIRF microscopy. The Env trimer (PDB 4ZMJ) was fitted into the electron density map of the membrane-bound Env trimer (EMD-21412). Two click fluorophores (donor LD555-TTZ and acceptor LD655-TTZ) were site-specifically introduced at $S401^{ncAA}$ and $R542^{ncAA}$ of a single protomer (gp120 in cyan, gp41 in pink; wild-type protomers in gray). Labeling sites are shown as green and red spheres, respectively. (**F**) Fluorescence emission spectra of HIV-1_{Q23} virions carrying click-labeled Env_{BG505} $S401^{ncAA}$ $R542^{ncAA}$, showing LD555 and LD655 signals from dual-color virions (solid cyan) compared with spectra from single-color-labeled virions (dashed lines). (**G**) Representative donor (green) and acceptor (red) fluorescence traces and corresponding FRET efficiency trajectories (blue) with hidden Markov modeling (HMM) idealization (magenta), from two individual ligand-free HIV-1_{Q23} virions carrying Env_{BG505} S401* R542* (left and right panels). The black arrow marks single-step photobleaching. Three FRET-populated states are indicated by color-coded bands.

The online version of this article includes the following source data and figure supplement(s) for figure 1:

Source data 1. PDF file containing uncropped western blot gel images for ***Figure 1B***, indicating the relevant bands clearly labeled.

Source data 2. Original files for western blot analysis in ***Figure 1B***.

Source data 3. Excel file containing the raw data used for the analysis in ***Figure 1D, F, G***.

Figure supplement 1. Primary structures of Env with a pair of dye-attached positions indicated on BG505 for single-molecule Förster Resonance Energy Transfer (smFRET) studies in ***Figure 1A***.

Figure supplement 2. Amber suppression and click-labeling strategy for preparing HIV-1_{Q23} Env_{BG505} virions for single-molecule Förster Resonance Energy Transfer (smFRET).

Figure supplement 3. Dual-amber suppression efficiency of HIV-1_{Q23} Env_{BG505} $S401^{TAG}$ $R542^{TAG}$, infectivity before and after labeling, and particle size distribution of the resulting virions.

Figure supplement 3—source data 1. Excel file containing the raw data used for the analysis in ***Figure 1—figure supplement 3***.

Figure supplement 4. Biophysical fluorescence properties of functionalized fluorophores and single-color-labeled Env_{BG505} HIV-1_{Q23} $S401^{ncAA}$ $R542^{ncAA}$ virions.

Figure supplement 4—source data 1. Excel file containing the raw data used for the analysis in ***Figure 1—figure supplement 4***.

incorporated into amber-free HIV-1_{Q23} virions, with no detectable Env in non-suppression controls (***Figure 1B***). Viral particle shape and size distributions were similar to wild-type, as revealed by cryo-ET, negative staining, and nanoparticle tracking analysis (***Figure 1C***, ***Figure 1—figure supplement 3C, D***). A quantitative analysis of capsid morphology, Env spike incorporation, and the proportion of immature particles would be more informative. However, we reason that such analyses would require a substantially larger cryoET dataset, which is beyond the scope of the present smFRET-focused study of Env conformational dynamics.

The ncAA-incorporated virions also exhibited neutralization sensitivities comparable to WT when tested against trimer-specific bNAbs, including PG16 (apex-directed; ***Walker et al., 2009***) and PGT151 (gp120–gp41 interface-directed; ***Blattner et al., 2014***; ***Figure 1D***). Of note, these validations were performed using virions generated entirely from dual-amber-tagged Env constructs. Together, these results (***Figure 1B–D***, ***Figure 1—figure supplement 3***) confirm proper Env expression, particle size, and preserved antigenicity, demonstrating that ncAA-incorporated Env is properly presented on intact virions and retains functional competence, and that click labeling does not affect virion infectivity. After functional validations and prior to single-molecule studies (***Figure 1E***), we performed ensemble-level spectral characterization. Dually labeled virions with donor and acceptor fluorophores exhibited well-separated excitation and emission profiles, and single-color-labeled control virions displayed the expected single-emission signatures consistent with those of free dyes, confirming specific fluorophore conjugation (***Figure 1F***, ***Figure 1—figure supplement 4***).

Real-time visualization of global CD4-associated opening of native virus Env from two structural perspectives

We next performed smFRET imaging of fluorescently labeled Env trimers on intact virions using a lab-customized prism-based TIRF microscope (***Figure 1E***). To optimize conditions for monitoring single FRET-labeled protomers, virions were generated by co-transfecting amber-free wild-type and $S401^{TAG}$ $R542^{TAG}$ Env constructs at a ratio based on the suppression efficiency. Under these conditions, most virions remained wild-type and thus unlabeled following fluorophore conjugation. Post-labeled virions were immobilized on streptavidin-coated quartz slides via biotin–streptavidin interactions in

a quartz–coverslip flow cell. Among labeled particles, those carrying a single gp120 bearing LD555/LD655 pairs within an otherwise wild-type Env background could be identified and analyzed based on their FRET signals. Thus, smFRET imaging selectively detected virions with a single dual-labeled protomer among mostly wild-type Env trimers, of which similar experimental designs (see Methods for details) have been successfully applied in prior smFRET studies of Env and other viral spike proteins (***Munro et al., 2014***; ***Lee et al., 2024***; ***Das et al., 2018***; ***Das et al., 2020***; ***Lu et al., 2020***).

We analyzed hundreds of single-molecule trajectories that displayed anti-correlated donor and acceptor fluorescence intensity fluctuations, along with discrete single-step photobleaching events, as exemplified in ***Figure 1G*** (fluorescence, top panels) for ligand-free S401* R542*. These features confirmed that individual traces correspond to single Env trimers in motion. The resulting FRET efficiency trajectories (***Figure 1G***, bottom panels; FRET = FRET efficiency) report real-time conformational changes of individual Env trimers over their observable time period, until photobleaching occurred. Hidden Markov modeling (HMM) analysis (***McKinney et al., 2006***; ***Qin, 2004***) of these trajectories, which deconvoluted each into the most probable sequence of discrete FRET states, consistently resolved three well-separated FRET populations (***Figure 1G***): a low-FRET state with a mean value of ~0.1, an intermediate-FRET state with a mean of ~0.3, and a high-FRET state with a mean of ~0.55. This three-state model aligns well with our previous work and that of others (***Munro et al., 2014***; ***Herschhorn et al., 2016***; ***Ma et al., 2018***; ***Ao et al., 2024***; ***Lu, 2021***; ***Leonhardt et al., 2023***).

We assigned the newly observed FRET populations from the gp120–gp41 (S401–R542) axis, referencing the well-characterized states from the gp120 V1–V4 (N136–S401) axis (***Figure 2***, ***Figure 2—figure supplement 1***, ***Figure 2—figure supplement 2***, ***Supplementary file 1***). Previous smFRET studies (***Munro et al., 2014***; ***Herschhorn et al., 2016***; ***Ma et al., 2018***; ***Ao et al., 2024***; ***Lu, 2021***; ***Leonhardt et al., 2023***) using the referenced axis have shown that native Env on virions predominantly resides in the PT state, transitions through the prefusion-closed (PC) state, and fully opens into the CD4-bound open (CO) state (simplified in ***Figure 2A, B***, see ***Figure 2—figure supplement 1*** for details). Because FRET values depend on donor–acceptor distance and probe geometry, we mapped the probe sites onto closed and open Env trimers (***Figure 2C, D***) and next compared gp120–gp41 and gp120 V1–V4 profiles under matched conditions. This enabled confident assignment of FRET populations to pre-triggered (PT), PC, and CO.

To quantify those populations observed from the S401–R542 axis, we compiled the overall conformational landscape and calculated state occupancies under ligand-free and ligand-bound conditions (***Figure 2E, F***, ***Supplementary file 1***). FRET histograms generated from hundreds of trajectories and fit with three Gaussian distributions revealed three well-separated populations, with high-FRET predominating in the absence of ligand. Addition of soluble CD4 (sCD4) and the co-receptor-mimicking antibody 17b shifted the distribution toward the low-FRET population (***Figure 2F***, ***Figure 2—figure supplement 2***). Parallel smFRET measurements using the gp120 V1–V4 (N136*–S401*) probe pair (***Figure 2G, H***) yielded similar ligand-free and ligand-induced shifts despite differences in absolute FRET values. These results collectively enabled the confident assignment of the low-FRET (~0.1), intermediate-FRET (~0.3), and high-FRET (~0.55) populations to the CO, PC, and PT states, respectively. As FRET values are inversely proportional to donor–acceptor separation, the two dyes are expected to be further apart in the CO state than in the PC state. This expectation is supported by atomistic molecular dynamics simulations, which show that Env adopts a larger inter-dye distance in the CO state than in the PC state (***Figure 2—figure supplement 3***). Together, these results suggest the gp120–gp41 probe pair as a reliable reporter of Env conformational dynamics and CD4-associated opening. The three-state model consistently provided the simplest and most probable explanation for both our current data and previous studies (***Munro et al., 2014***; ***Ma et al., 2018***; ***Lee et al., 2024***; ***Ao et al., 2024***; ***Lu et al., 2019a***). The consistency of these shifts across probe-pair positions provides compelling evidence that trimer opening is an intrinsic dynamic property of Env. It undergoes global conformational changes upon engaging with sCD4 and 17b, independent of the observed smFRET structural perspective.

To align our nomenclature with that of previous studies (***Munro et al., 2014***; ***Herschhorn et al., 2016***; ***Ma et al., 2018***), the PT state corresponds to previously designated State 1, the PC state corresponds to the symmetric State 2 (which the SOSIP-based soluble Env primarily adopts; ***Lu et al., 2019a***), and the CO state corresponds to the fully open State 3. Additional conformational substates, including partially open or asymmetric Env trimers, or other low-abundance substates, may exist and

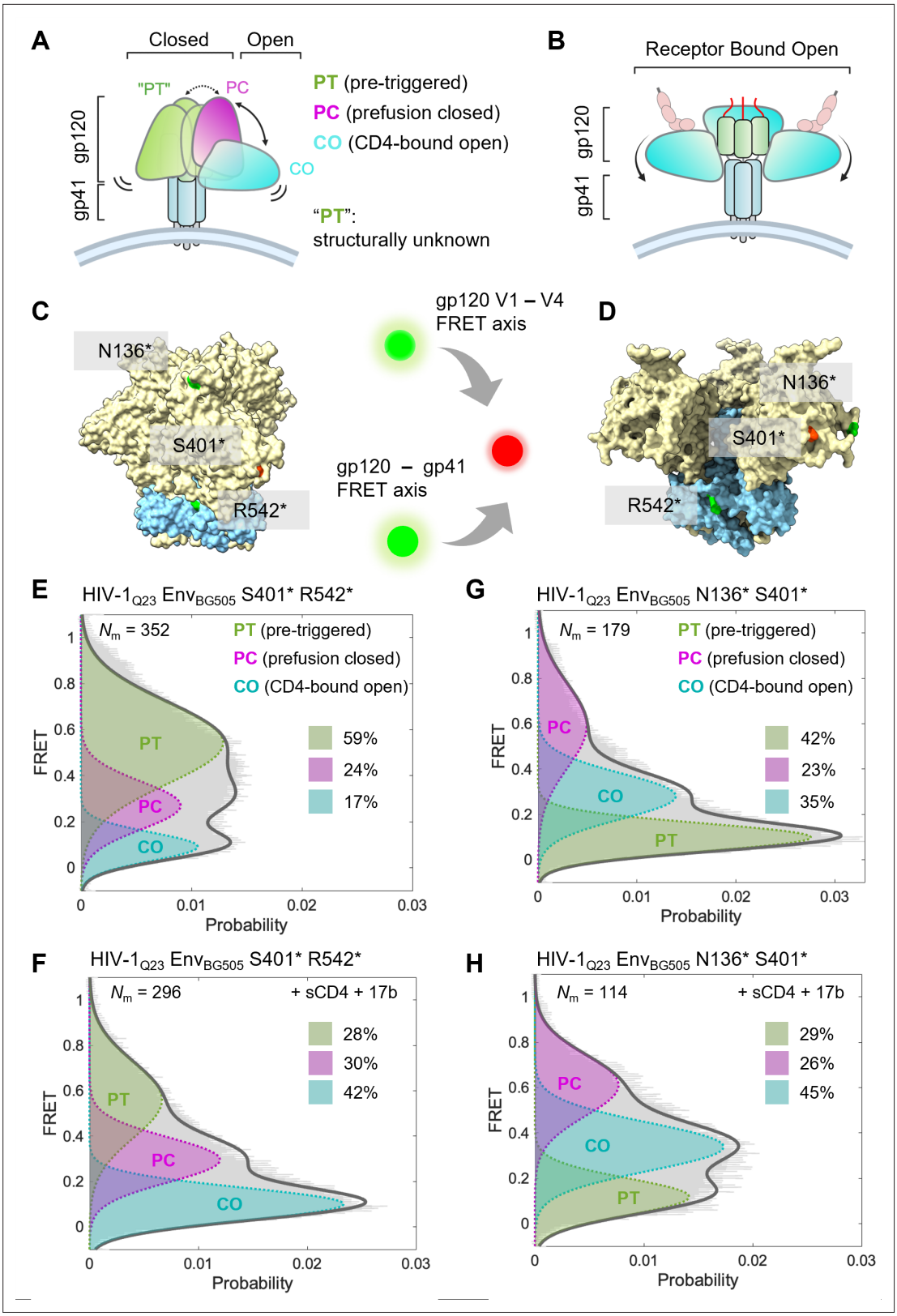


Figure 2. Single-molecule Förster Resonance Energy Transfer (smFRET) observation of global conformational opening of Env trimer from gp120–gp41 and gp120 V1V4 structural perspectives. (**A, B**) Schematic models of Env conformational states. (**A**) gp120 adopts three major conformations: 'PT' (pre-triggered, structurally unknown), PC (prefusion-closed), and CO (CD4-bound open), shown for a single protomer within the trimer, with the other two protomers remaining in the PT state. (**B**) Fully open Env trimer schematic showing all three gp120 subunits in the CD4-bound state. (**C, D**) Structural

Figure 2 continued on next page

Figure 2 continued

visualization of Env conformations from two smFRET probe perspectives. Env trimers in the PC (**C**, PDB #4TVP) and fully open (**D**, PDB #5VN3) states are shown with probe positions highlighted: gp120–gp41 (S401* R542*) and gp120 V1V4 (N136* S401*). FRET histograms of Env_{BG505} S401* R542* (gp120–gp41 perspective) on native virions without ligand (**E**) or with soluble CD4 (sCD4) plus the co-receptor-mimicking antibody 17b (**F**). Ligand-free Env samples three primary conformational states (as in panel A), whereas sCD4 and 17b stabilize the fully open conformation (as in panel B). Here and elsewhere, N_m indicates the number of FRET trajectories – molecules that were used to construct the histogram and were fit to the sum of three Gaussian distributions (see ***Supplementary file 1***). State occupancies are reported as percentages. (**G, H**) Validation from the gp120 V1V4 perspective using Env_{BG505} N136* S401*. FRET histograms confirm a conformational shift toward the open-dominated population.

The online version of this article includes the following source data and figure supplement(s) for figure 2:

Source data 1. Excel file containing the raw data used for the analysis in ***Figure 2E–H***.

Figure supplement 1. Relative protomer movements in symmetric PT, PC, and CO Env trimers.

Figure supplement 2. Representative traces of Env predominantly in the open conformation.

Figure supplement 2—source data 1. Excel file containing the raw data used for the analysis in ***Figure 2—figure supplement 2***.

Figure supplement 3. Molecular dynamics simulation of dye-conjugated soluble Env trimer in prefusion-closed state and CD4-bound state.

Figure supplement 3—source data 1. Excel file containing the raw data used for the analysis in ***Figure 2—figure supplement 3***.

may be resolved under different experimental or triggering conditions. For example, previous work showed that asymmetric intermediate conformations can be resolved using a heterotrimer design containing mixtures of wild-type and CD4-binding-deficient D368R protomers, where the State 2 FRET signal can originate from an unliganded protomer while the remaining one or two protomers are CD4-bound and open (***Ma et al., 2018***). In the present study, we did not use such a heterotrimeric design. Therefore, although our labeling strategy reports the major conformational populations of Env, it cannot unambiguously distinguish protomer asymmetric states, such as trimers with only one or two gp120 molecules open. Evidence from current and previous studies (***Munro et al., 2014***; ***Herschhorn et al., 2016***; ***Ma et al., 2018***; ***Ao et al., 2024***; ***Lu et al., 2019a***) strongly supports the presence of three primary states of virus-associated Env, with additional substates that can be resolved under specific triggering conditions (***Alsahafi et al., 2019***; ***Lee et al., 2024***; ***Richard et al., 2025***). Accordingly, the three Gaussian models used here represent the three predominant conformational populations under our experimental conditions.

Allosteric stabilization of Env in the PC state by gp120–gp41 interface and FP bNAbs

We next investigated how gp120–gp41 interface and FP bNAbs influence Env conformational dynamics. To this end, we performed smFRET analysis of fluorescently labeled Env_{BG505} S401*–R542* trimers on intact virions in the presence of 8ANC195 (***Scharf et al., 2014***), VRC34 (***Thakur et al., 2025***; ***Kong et al., 2016***), or PGT151 (***Blattner et al., 2014***; ***Figure 3***, ***Figure 3—figure supplement 1***). Sequences of heavy and light chains of antibodies used in this study are provided in ***Supplementary file 2***. Dose–response neutralization curves confirmed potent yet distinct activity of all three bNAbs against $HIV\text{-}1_{Q23}$ Env_{BG505} virions (***Figure 3A***, left). The three antibodies engage distinct epitopes at the gp120–gp41 subunit interface (***Figure 3A***, right; ***Thakur et al., 2025***; ***Blattner et al., 2014***; ***Scharf et al., 2014***; ***Kong et al., 2016***): 8ANC195 and PGT151 make extensive contacts with both gp41 and gp120, whereas VRC34 binds predominantly to the N-terminal region of the FP. These distinct binding modes likely result in differential effects on the conformational landscape of native Env, motivating smFRET studies to uncover their impact on Env dynamics.

We compiled FRET histograms (***Figure 3B–D***), which revealed antibody-specific effects on Env conformational sampling. Histograms were constructed from $\boldsymbol{N}_m$ of smFRET trajectories, as indicated in each plot. Representative examples (***Figure 3—figure supplement 1***) displayed characteristic anti-correlated donor–acceptor intensity fluctuations and state-to-state transitions, consistent with conformational sampling between PT, PC, and CO states. In the presence of 8ANC195, Env displayed a modest redistribution from the high-FRET PT state (occupancy decreased from 59% to 45%) toward the intermediate-FRET PC (24% to 32%) and low-FRET CO (17% to 23%) states. By contrast, VRC34 and PGT151 induced more pronounced shifts, resulting in PC state dominance (42% and 47%, respectively) and a marked reduction in PT occupancy (54–34%). We further summarized state occupancies under antibody-incubated conditions, in reference to those for ligand-free and CD4/17b-incubated

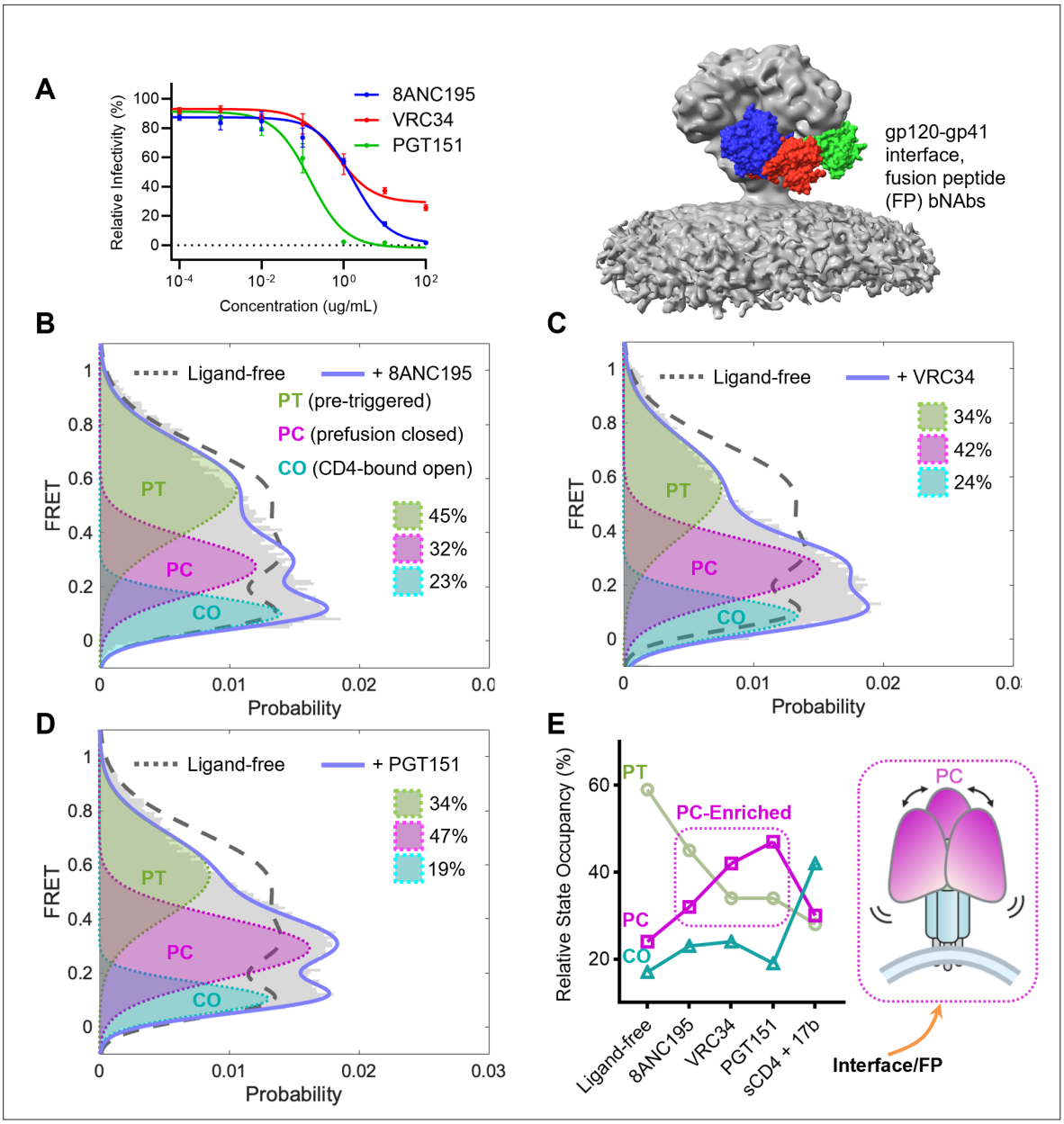


Figure 3. Stabilization of HIV-1 Env in the prefusion-closed (PC) state by gp120–gp41 interface or fusion peptide (FP) bNAbs. (**A**) Dose–response neutralization curves (left, $n = 4$) of HIV-1_{Q23} Env_{BG505} by the gp120–gp41 interface or FP bNAbs 8ANC195, VRC34, and PGT151, with binding epitopes mapped onto the membrane-bound Env trimer (EMD-21412, right). (**B**) FRET histogram of HIV-1_{Q23} Env_{BG505} S401* R542* in the presence of 8ANC195, overlaid with ligand-free Env (dashed gray), showing modest conformational shifts toward downstream states. FRET histograms for VRC34 (**C**) and PGT151 (**D**), as in (**B**), revealing redistribution of Env populations from pre-triggered (PT) to PC state dominance. (**E**) Line graph showing relative state occupancy of Env under different antibody conditions, demonstrating progressive enrichment of the PC state by 8ANC195, VRC34, and PGT151.

The online version of this article includes the following source data and figure supplement(s) for figure 3:

Source data 1. Excel file containing the raw data used for the analysis in ***Figure 3***.

Figure supplement 1. Representative single-molecule Förster Resonance Energy Transfer (smFRET) traces of HIV-1_{Q23} EnvBG505 S401* R542* with gp120–gp41 interface or fusion peptide bNAbs.

Figure supplement 1—source data 1. Excel file containing the raw data used for the analysis in ***Figure 3—figure supplement 1***.

conditions, using line graph (***Figure 3E***) derived from quantitative model fitting of FRET histograms with constrained three-state Gaussian models (***Supplementary file 1***). These analyses revealed allosteric enrichment of the PC state across the antibody panel (***Figure 3E***, inset model plot), with the strongest stabilization observed for PGT151 (47%). Ligand-induced stabilization, as revealed by smFRET here, reflects a redistribution of the conformational ensemble while preserving the intrinsic dynamic nature of Env. These results suggest that gp120–gp41 interface and FP-targeting bNAbs remodel the Env conformational landscape by allosterically shifting the distribution toward the PC state along the gp120 opening pathway.

MPER-directed bNAbs allosterically stabilize the PC state, while 10E8.4/iMab exerts a dual effect by also promoting the CO state

We next examined how MPER-directed bNAbs DH511.2_K3 (***Williams et al., 2017***), VRC42, (***Krebs et al., 2019***), and the bispecific antibody 10E8.4/iMab influence Env conformational dynamics on native virions. Sequences are listed in ***Supplementary file 2***. All antibodies potently neutralized HIV-1_{Q23} Env_{BG505}, with the bispecific engineered 10E8.4/iMab, (***Huang et al., 2016***; ***Padte et al., 2018***) which combines a variant of the 10E8 antibody with the CD4 receptor-targeting antibody iMab, exhibiting exquisite potency (***Figure 4A***, left). Their distinct binding epitopes, located distal to the gp120 opening apex, were defined from Env–bNAb complex structures solved with truncated gp41 peptide constructs and mapped to the MPER region of Env (***Figure 4A***, right), which lies adjacent to the viral membrane. DH511.2_K3 is a 10E8-like antibody, (***Williams et al., 2017***) and VRC42 shares similar binding epitopes with the 4E10 antibody (***Krebs et al., 2019***). For 10E8.4/iMab, neither the structural details of its complex with Env nor its impact on Env dynamics has been defined, although the structure of 10E8 itself with MPER peptide has been determined (***Huang et al., 2012***). In light of this, we used smFRET to directly observe, from the gp120-gp41 axis (S401* R542*), how these antibodies allosterically remodel Env conformational distributions in the native viral context.

Two MPER-directed bNAbs exhibited a preference for the intermediate-FRET state, and thus a prevalent residence in the PC state observed from FRET histograms (***Figure 4B, C***). The conformational redistribution from PT to PC dominance for DH511.2_K3 (***Figure 4B***) and VRC42 (***Figure 4C***) suggests that MPER engagement allosterically restricts the trimer apex from fully opening by stabilizing the base where the binding epitopes reside. Otherwise, one would expect an increase in the CO state rather than no notable change. The result is somewhat unexpected. We initially hypothesized that Env would need to adopt a more open conformation to permit bNAb access to the sterically restricted epitopes near the viral membrane. The results, nevertheless, are consistent with those obtained from cryo-EM structures using the Env ectodomain or the isolated MPER domain (***Williams et al., 2017***; ***Krebs et al., 2019***). There are three plausible mechanisms by which MPER-directed antibodies could access their epitopes: (1) partial or full gp120 opening to relieve steric constraints on gp41, (2) trimer tilting relative to the viral membrane, and (3) local membrane bending or curvature. Although our initial hypothesis favored some degree of gp120 opening, the observed stabilization of the PC state suggests that MPER accessibility may arise through trimer tilting or membrane deformation, in line with a recent observation of membrane-coupled Env trimer tilting on virions (***Croft et al., 2026***).

The bivalent 10E8.4/iMab, strikingly, induced a distinct conformational response of Env on virions. It stabilized Env in both PC and CO states, with the latter predominating at the cost of the PT state (***Figure 4D***). FRET histograms revealed a redistribution beyond PC toward the largest increase in CO-state sampling (***Figure 4D***). When combined with sCD4 and 17b, 10E8.4/iMab further amplified this shift, driving Env even further into the CO state with reduced sampling of other conformations (***Figure 4E***). Therefore, unlike the other two monovalent MPER antibodies that primarily stabilize the PC state, the results indicate that 10E8.4/iMab exerts a dual effect (***Figure 4F–I***), favoring both the PC and, more profoundly, the CO states at the expense of the PT state. The order of antibody presentation in quantitative results and comparisons of state occupancies (***Figure 4F–H***) was intentionally arranged to illustrate this continuum of Env opening, highlighting the gradual redistribution of state occupancies from MPER-bNAb-stabilized closed conformations to 10E8.4/iMab- and sCD4/17b-driven open states.

We next performed smFRET of Env in the presence of 10E8.4 and iMab individually to examine their separate conformational effect on the virus-associated Env (***Figure 4—figure supplement 1***). We found that 10E8.4 behaves similarly to other MPER-directed antibodies in enriching the PC state,

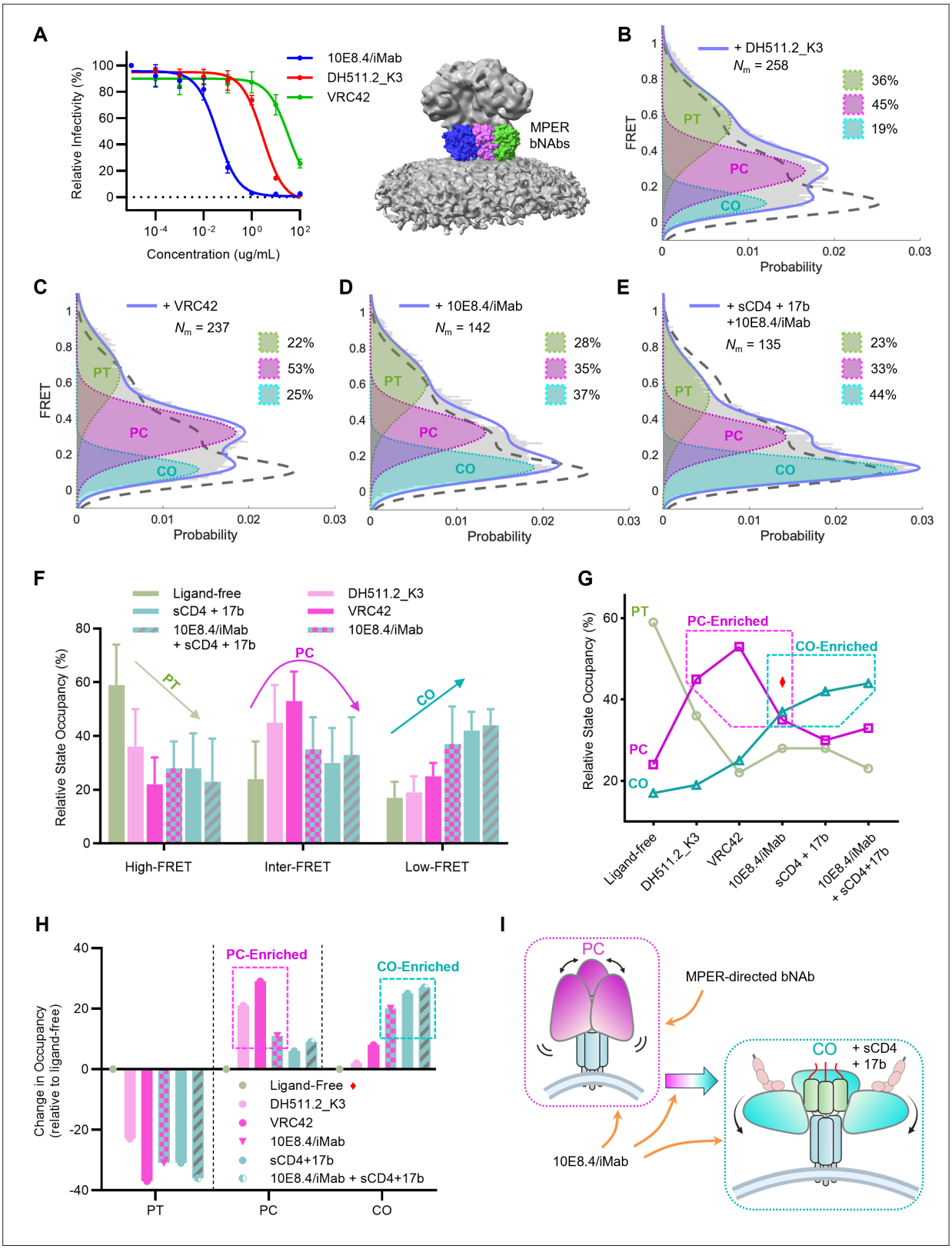


Figure 4. Membrane-proximal external region (MPER)-directed bNAbs enrich Env in the prefusion-closed (PC) state, while 10E8.4/iMab also enriches Env in the CD4-bound open (CO) state. (**A**) HIV-1 neutralization by MPER-directed antibodies DH511.2_K3 and VRC42, and 10E8.4/iMab. Left: neutralization curves; right: MPER-binding epitopes on Env. n = 4. FRET histograms of Env_{BG505} S401* R542* in the presence of DH511.2_K3 (**B**) or VRC42 (**C**). These MPER-directed bNAbs shift Env toward dominance of the PC state. The FRET histogram for Env with sCD4 and 17b (dashed gray) was

Figure 4 continued on next page

Figure 4 continued

included in each plot for reference. Single-molecule Förster Resonance Energy Transfer (smFRET) results for bi-valent 10E8.4/iMab alone (**D**), which shifts Env further downstream along the opening pathway with a broad range across PC and CO, and with sCD4 and 17b (**E**), which further stabilizes Env in the open CO state. Bar graph (**F**), mean ± SEM, and line graph (**G**) showing relative state occupancy of Env under different antibody-binding conditions, demonstrating shifts from pre-triggered (PT) to PC with MPER bNAbs, and progression toward CO with 10E8.4/iMab alone or combined with sCD4 and 17b. (**H**) Bar graph of changes in state occupancy of Env exerted by MPER antibodies relative to ligand-free. (**I**) A derived schematic summarizing smFRET results of preferential conformations of Env targeted by MPER-directed bNAbs and 10E8.4/iMab.

The online version of this article includes the following source data and figure supplement(s) for figure 4:

Source data 1. Excel file containing the raw data used for the analysis in ***Figure 4***.

Figure supplement 1. 10E8.4 enriches Env in the PC state, while iMab itself has no effect on Env conformations.

Figure supplement 1—source data 1. Excel file containing the raw data used for the analysis in ***Figure 4—figure supplement 1***.

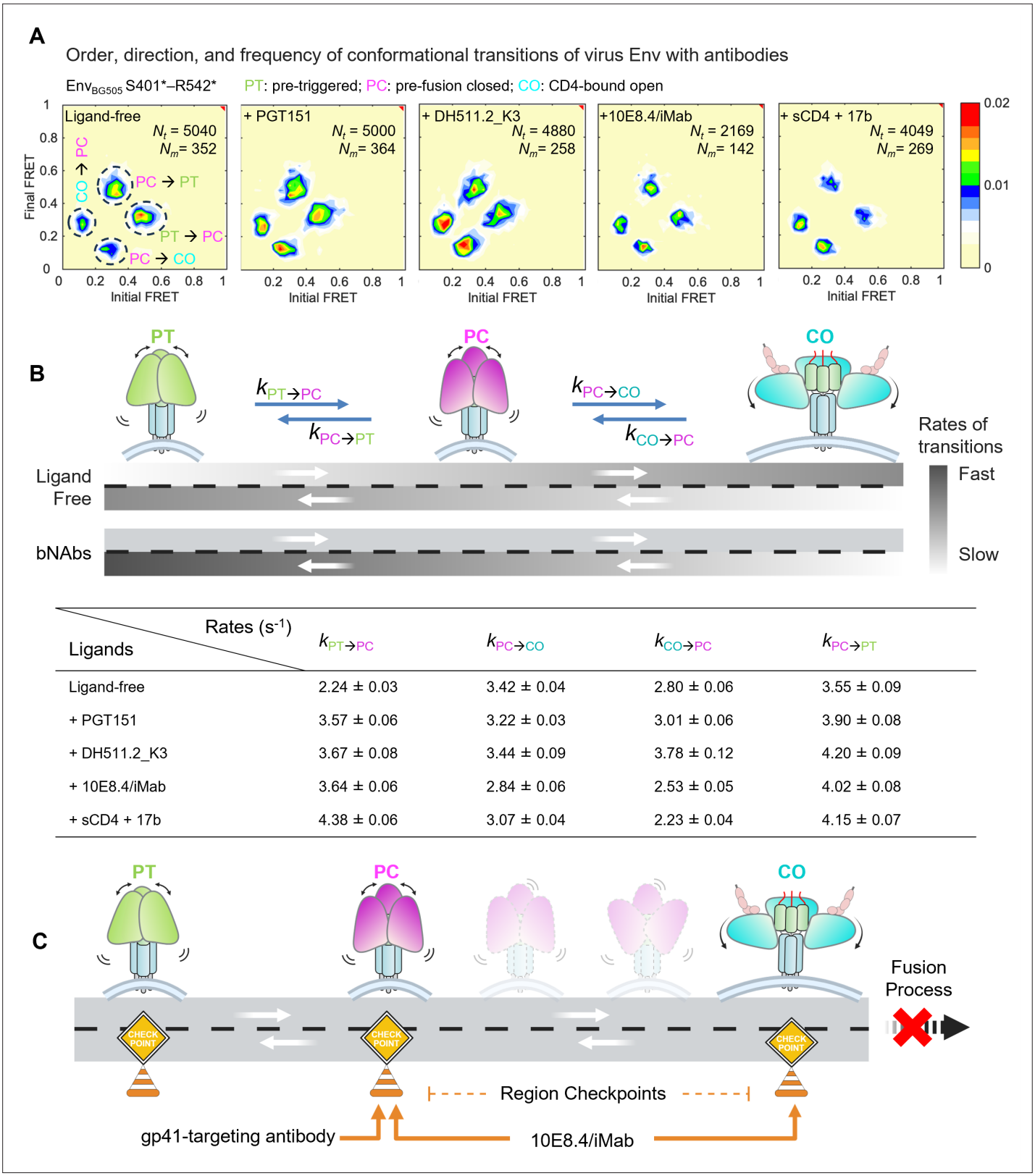
whereas iMab alone does not appear to have a notable effect on the conformational propensity of Env (***Figure 4—figure supplement 1***).

The distinct conformational responses induced by 10E8.4/iMab are intriguing and unexpected, given that the 10E8 arm behaves similarly to other MPER-directed antibodies, and the iMab arm engages CD4 on the host membrane (and thus is not expected to interact with Env trimer). Notably, this effect of favoring the CO state was observed even in the absence of CD4 or the host membrane context. The unique neutralization of 10E8.4/iMab is reminiscent of CD4-induced opening of the spike, and indeed, the binding of MPER-directed antibodies has been shown to synergize with that of CD4 (***Ruprecht et al., 2011***; ***Foulkes et al., 2025***), as explored further in the Discussion section.

Antibodies shift Env transition frequencies with limited effects on rates while preserving the opening pathway

To investigate how antibodies influence Env dynamics beyond overall conformational distributions and steady-state occupancies, we analyzed single-molecule trajectories to extract state-to-state transitions and quantify their kinetics (Methods). Transition density plots (TDPs) were generated by plotting the initial versus final FRET values for every detected transition, with color intensity reflecting the relative frequency of transitions (transitions per second) (***Figure 5A***). These plots report which transitions occur and how often, with the total number of transitions (N_t) and molecules analyzed (N_m, the same molecules used for the FRET histograms and occupancy analysis) indicated on each plot. These TDPs revealed antibody-dependent redistribution of state-to-state transitions: interface/FP bNAbs (such as PGT151) and MPER bNAbs (such as DH511.2_K3) enriched transitions into and within the intermediate-FRET PC state, whereas 10E8.4/iMab and sCD4/17b increased transitions leading toward the low-FRET CO state from both PT and PC. The expected set of allowable transitions between PT and PC, between PC and CO, and rarely between PT and CO was preserved under all conditions (***Figure 5A***), suggesting that the overall order and directionality of Env state-to-state transitions remain unchanged.

To determine whether these occupancy shifts were accompanied by changes in transition kinetics, we constructed survival probability plots for each FRET-defined state (***Figure 5—figure supplement 1***). Dwell times for molecules in each state prior to a transition were pooled, and exponential functions were fit to the resulting distributions to derive weighted-average rates for transitions between allowable conformations. These rate constants, which fall on the scale of seconds, were summarized as a directional connectivity schematic and a numerical table (***Figure 5B***). This analysis revealed only modest antibody-induced changes in transition rates, suggesting that the primary effect of the tested antibodies is to allosterically redistribute the frequencies of state sampling rather than fundamentally rewire the intrinsic kinetics of Env motion. Together with the TDPs, these results demonstrate that antibodies shift transition frequencies while preserving the overall network of allowable transitions, leaving the canonical opening pathway intact.



Ligands \ Rates (s^{-1})	$k_{PT→PC}$	$k_{PC→CO}$	$k_{CO→PC}$	$k_{PC→PT}$
Ligand-free	2.24 ± 0.03	3.42 ± 0.04	2.80 ± 0.06	3.55 ± 0.09
+ PGT151	3.57 ± 0.06	3.22 ± 0.03	3.01 ± 0.06	3.90 ± 0.08
+ DH511.2_K3	3.67 ± 0.08	3.44 ± 0.09	3.78 ± 0.12	4.20 ± 0.09
+ 10E8.4/iMab	3.64 ± 0.06	2.84 ± 0.06	2.53 ± 0.05	4.02 ± 0.08
+ sCD4 + 17b	4.38 ± 0.06	3.07 ± 0.04	2.23 ± 0.04	4.15 ± 0.07

Figure 5. Kinetic analysis of Env transitions exerted by gp41-directed antibody and 10E8.4/iMab, and an integrative model depicting allosteric control across conformational states. (**A, B**) gp41-directed antibody and the bispecific 10E8.4/iMab alter Env transition frequencies with slight effects on kinetic rates while preserving the opening pathway. (**A**) Transition density plots (TDPs) showing the order, directionality, and frequency of Env conformational transitions in the presence of representative bNAbs. Each TDP plots the initial versus final FRET value for every detected transition, with color intensity

Figure 5 continued on next page

Figure 5 continued

indicating the relative frequency of those transitions (transitions per second). N_t = total number of transitions from N_m (total number of molecules), indicated on each plot. These plots reveal antibody-dependent redistribution of state sampling among pre-triggered (PT), prefusion-closed (PC), and CD4-bound open (CO) conformations. (**B**) Schematic (top) and table (bottom) summarizing transition rates between allowable Env conformations in the presence of interface/fusion peptide (FP), membrane-proximal external region (MPER), and 10E8.4/iMab antibodies. (**C**) Integrative working model of gp41 antibody-mediated allosteric control of Env conformational states. Native Env on virions transitions through three primary states (PT, PC, and CO) along the opening pathway toward fusion, depicted as sequential checkpoints along the opening/fusion road targeted by antibodies. Most gp41-directed bNAbs act preferentially at the PC checkpoint, whereas 10E8.4/iMab can act at both PC and CO. The MPER- and CD4-binding arms of 10E8.4/iMab may function as a mechanical brace, restraining Env from breaking free at PC, CO, and the secondary checkpoints between them, which could explain its superior potency.

The online version of this article includes the following source data and figure supplement(s) for figure 5:

Figure supplement 1. Survival probability plots used to estimate transition rates among Env conformations.

Figure supplement 1—source data 1. Excel file containing the raw data used for the analysis in ***Figure 5—figure supplement 1***.

Discussion

Two modes of neutralization via allosteric control of Env dynamics across distinct conformational checkpoints

In this study, we demonstrate that gp41-directed bNAbs exert long-range allosteric control of Env dynamics through two different conformational outcomes. Most bNAbs targeting the gp120–gp41 interface, FP, and MPER stabilize the PC state and restricted sampling of the PT conformation. In contrast, the bispecific 10E8.4/iMab, a promising therapeutic currently in clinical trials, exerts a dual effect by also stabilizing the CO state. These findings lead to our current working model (***Figure 5C***). The native Env on virions transitions through three primary conformational checkpoints, from PT through PC to CO, along the opening pathway toward fusion. Multiple secondary checkpoints likely exist between the PC and CO states. Whereas most gp41-directed bNAbs act primarily at the PC checkpoint, 10E8.4/iMab can engage both PC and CO checkpoints and may also act at substates in between.

These conformational controls over Env reveal two dynamic modes of neutralization: (1) allosteric stabilization of the PC state, and (2) premature triggering into the open state. Regarding the second mode, associated with 10E8.4/iMab, we cannot exclude the possibility that the CD4-targeting arm enhances or stabilizes binding of the 10E8.4 arm to Env, thereby improving access to its epitope in the CD4-bound conformation. Premature triggering of global conformational changes and localized epitope binding are not mutually exclusive; rather, they may coexist. In either case, both modes reflect the intrinsic allosteric regulation of Env, where perturbations at one site, such as antibody binding or a single amino acid substitution, can propagate across the trimer to stabilize or destabilize distant domains. Prior studies have shown that even a single or a few substitutions can reconfigure distal structural elements (***Herschhorn et al., 2016***, ***Herschhorn et al., 2017***, ***Henderson et al., 2020***, ***Chatterjee et al., 2025***, ***Bennett and Henderson, 2021***), underscoring the remarkable sensitivity of Env to allosteric perturbation.

These two modes form a continuum, with different antibodies shifting Env among checkpoints along the opening pathway (***Figure 5C***). Such dynamic control likely underlies the exceptional potency of some antibodies, such as the bispecific 10E8.4/iMab, by broadening the range of neutralized conformations while reducing opportunities for viral escape across multiple conformational checkpoints.

Striking Env opening by 10E8.4/iMab in the absence of CD4

The finding that MPER-directed bNAbs stabilize the PC state also suggests that MPER accessibility on gp41 does not necessarily require trimer opening, which was unexpected, as discussed in the Results section. Even more surprising, however, was the observation that 10E8.4/iMab stabilizes the CO state in addition to the PC state, despite the absence of soluble or membrane-associated CD4.

We suspect that the two binding arms of 10E8.4/iMab may act like a molecular (mechanical) brace on a hinge, limiting Env escape at and between these two primary conformational checkpoints (***Figure 5C***). This effect likely broadens the range of conformational states and substates accessible to neutralization, which could explain its superior neutralizing abilities in both potency and breadth. Whether 10E8.4/iMab can target multiple unknown substates or secondary checkpoints (***Figure 5C***)

of Env along the opening trajectory remains to be clarified; however, two recent integrative studies provide relevant context. Using collective molecular dynamics, one computational study revealed a previously overlooked neutralization-relevant occluded-intermediate state between PC and CO that emerged in the presence of one of four specific bNAbs (***Lee et al., 2024***). This newly identified state was further supported by smFRET analyses, which showed reproducible conformation-related shifts validated through statistical evaluation of multiple models (***Lee et al., 2024***). Another recent cryo-EM study identified several open intermediates with varying degrees of FP accessibility, induced by bNAb VRC34 under different open-triggering conditions (***Thakur et al., 2025***). Again, the existence of these new intermediates was supported mechanistically by smFRET results using new probes performed under the same conditions (***Thakur et al., 2025***). Of note, these newly identified conformations or states between PC and CO were not previously observed in initial cryo-EM (***Kong et al., 2016***; ***Banach et al., 2023***) or smFRET (***Kong et al., 2016***) of Env–VRC34. These observations are encouraging, as they underscore the likelihood that 10E8.4/iMab targets a broad range of Env conformations, including PC, CO, and even currently uncharacterized 'hidden' Env conformations. Future structural investigations, particularly high-resolution studies of 10E8.4/iMab bound to membrane-associated Env and membrane-embedded CD4, could provide deeper mechanistic insights into how distinct binding modes mediate allosteric regulation and inhibit fusion through conformational control, trimer tilting, or membrane deformation.

Underappreciated transition kinetics of Env dynamics

An additional mechanistic insight, often underappreciated, is that antibody-induced conformational redistribution occurred without major rewiring of the intrinsic opening pathway (***Figure 5A, B***). Our kinetic analysis reveals that the overall transition network and directionality (PT ↔ PC ↔ CO), which describe the progression from PT to PC and onward to CO, remain preserved. Antibody effects were primarily reflected in shifts in transition frequencies and state occupancies, with only modest changes in transition rates. This suggests that antibodies primarily act by stabilizing or destabilizing specific states within the preexisting pathway, rather than creating alternative routes. Such long-range allosteric modulation provides a mechanism for neutralization while maintaining the intrinsic connectivity of Env dynamics.

Coherent mechanistic landscape linking Env structures and dynamics to neutralization

The observed conformational redistributions of Env by 8ANC195, VRC34, PGT151, DH511.2_K3, VRC42, and 10E8.4/iMab are mechanistically consistent with structural studies that mapped Env–antibody epitopes on predominantly closed conformations (***Thakur et al., 2025***; ***Blattner et al., 2014***; ***Scharf et al., 2014***; ***Kong et al., 2016***; ***Williams et al., 2017***; ***Krebs et al., 2019***; ***Huang et al., 2012***; ***Kwon et al., 2016***). They are also in line with previous smFRET studies using probes confined to gp120 (***Thakur et al., 2025***; ***Ao et al., 2024***; ***Lu et al., 2019a***; ***Kong et al., 2016***), as well as molecular virology studies examining neutralization sensitivity or resistance in tier-level viruses or those with Env modifications (***Ivan et al., 2019***; ***Ruprecht et al., 2011***; ***Foulkes et al., 2025***; ***Parthasarathy et al., 2024***; ***Flemming et al., 2018***). Structural analyses have revealed how Env–antibody complexes neutralize through direct binding, identifying atomic footprints and steric blockades that prevent CD4 or co-receptor engagement or insert into fusion-critical elements to block entry (***Thakur et al., 2025***; ***Blattner et al., 2014***; ***Scharf et al., 2014***; ***Kong et al., 2016***; ***Williams et al., 2017***; ***Krebs et al., 2019***; ***Huang et al., 2012***; ***Kwon et al., 2016***). These static structural snapshots of bNAb–Env complexes, primarily captured with engineered or truncated Env in the closed conformation, align with the PC dominance observed in this study. Previous smFRET analyses of PGT151 and VRC34 with probes restricted to gp120 (***Thakur et al., 2025***; ***Ao et al., 2024***; ***Lu et al., 2019a***; ***Kong et al., 2016***) revealed their preferential recognition of PC, distinct from the PT state. Our updated smFRET approach, using dual bioorthogonal click labeling across the gp120–gp41 structural axis, reinforces the finding of PC stabilization and provides additional insight into transition kinetics. The smFRET characterization of 8ANC195, VRC42, DH511.2_K3, and 10E8.4/iMab presented here is, to our knowledge, the first of its kind, revealing Env conformational responses and transition kinetics. Molecular virology studies have also reported correlations between the neutralization sensitivity of gp120- and gp41-directed bNAbs and the conformational flexibility, and, in some cases, the degree of opening

or closing of Env trimers (***Ivan et al., 2019***;***Ruprecht et al., 2011***;***Foulkes et al., 2025***;***Parthasarathy et al., 2024***;***Flemming et al., 2018***). Our smFRET data, which capture Env conformational distributions and bNAb-induced shifts, reveal intrinsic conformational flexibility consistent with these studies in principle. In particular, one MPER-directed bNAb, 10E8.4/iMab, can open the spike in a manner similar to CD4, consistent with other experiments showing that MPER and CD4 binding synergize (***Ruprecht et al., 2011***; ***Foulkes et al., 2025***).

Overall, our results introduce dynamic and kinetic dimensions to the neutralization landscape within the native viral context. Our data reveal the dynamic range of Env responses to antibody binding, highlighting the complementary aspects of structural stabilization and conformational plasticity in neutralization. These findings provide new mechanistic insights into neutralization by identifying how antibodies target Env on virions across multiple conformational checkpoints through mediating its conformational sampling probabilities, transition frequencies, and the trajectories it undergoes.

Complementary views from smFRET and structural studies in general

The smFRET analyses reveal that bNAb binding generally shifts the conformational equilibrium of Env rather than driving all trimers into a single structural state. Even in the presence of saturating ligands, substantial fractions of Env remain in alternative conformations, highlighting the intrinsic conformational heterogeneity of the native viral spike. This heterogeneity likely reflects both differences in ligand binding and the dynamic energy landscape of Env. In this regard, smFRET and structural methods provide complementary information. While cryo-EM and cryo-ET define the molecular architecture of individual conformational states, smFRET quantifies their relative populations and dynamic interconversion. The conformational ensembles observed by cryo-EM may also be influenced by factors such as conformation-dependent radiation sensitivity and the requirements of image classification, making low-abundance or highly dynamic states more difficult to recover. Together, these complementary approaches provide a more complete view of Env conformational dynamics than either method alone. The TDPs further illustrate how different ligands reshape the conformational landscape by altering both state occupancies and the transitions between them, rather than simply stabilizing a single static structure.

Limitations of this study

Several limitations should be acknowledged. Our smFRET studies were performed on virion-associated full-length Env, but in the absence of host membranes. This limits interpretation, as host lipid composition, membrane curvature, and host factors could influence Env dynamics and potentially contribute to neutralization. We did not capture the full conformational continuum, particularly downstream states after co-receptor engagement and gp41 refolding, which will require dual labeling of gp41 and host membranes together with complementary methods such as time-resolved cryo-EM or cryo-ET. Photobleaching of the donor and acceptor fluorophores within approximately 10 s of excitation limits the observation window for individual molecules. Technically, while smFRET provides millisecond-scale resolution of state sampling suitable for Env dynamics, very short-lived conformations remain underrepresented. Labeling at the gp120–gp41 axis was optimized to minimize perturbation, but chemical modifications could still influence local structural fluctuations normally below our detection threshold. The conformational effects of antibodies were examined in a single Env background (BG505, widely used and representative), although Env sequence diversity may modulate antibody-dependent effects. Finally, the link between Env dynamics and neutralization potency will require integration with in-depth structure–function analyses in a native context. Nevertheless, our findings refine the mechanistic understanding of antibody-mediated neutralization and reveal gp41 as a promising target for strategies that exploit the intrinsic allosteric vulnerabilities of Env.

Materials and methods

Key resources table

Reagent type (species) or resource	Designation	Source or reference	Identifiers	Additional information
Strain, strain background (*Escherichia coli*)	Stbl3	Invitrogen	Cat# C7373-03	

Continued on next page

Reagent type (species) or resource	Designation	Source or reference	Identifiers	Additional information
Cell line (*Homo sapiens*)	HEK293T	ATCC	Cat# CRL-3216 RRID:CVCL_0063	
Cell line (*Homo sapiens*)	TZM-bl	BEI resources	Cat# ARP-8129 RRID:CVCL_B478	
Antibody	HIV-1 gp120B (Sheep antiserum polyclonal)	BEI resources	Cat# ARP-288	WB (1:1000)
Antibody	PG16 (Human monoclonal)	BEI resources	Cat# ARP-12150	Virus neutralization assay (10 μg /ml)
Antibody	PGT151 (Human monoclonal)	Peter D Kwong Lab, NIH		smFRET (100 μg/ml)
Antibody	8ANC195 (Human monoclonal)	Peter D Kwong Lab, NIH		smFRET (100 μg/ml)
Antibody	VRC34 (Human monoclonal)	Peter D Kwong Lab, NIH		smFRET (100 μg/ml)
Antibody	VRC42 (Human monoclonal)	Peter D Kwong Lab, NIH		smFRET (100 μg/ml)
Antibody	DH511.2_K3 (Human monoclonal)	Priyamvada Acharya Lab, Duke University		smFRET (100 μg/ml)
Antibody	10E8.4 (Human monoclonal)	Peter D Kwong Lab, NIH		smFRET (100 μg/ml)
Antibody	iMab (Human monoclonal)	David D Ho Lab, Columbia University		smFRET (100 μg/ml)
Antibody	10E8.4/iMab (Human monoclonal)	David D Ho Lab, Columbia University		smFRET (100 μg/ml)
Antibody	17b (Human monoclonal)	Priyamvada Acharya Lab, Duke University		smFRET (100 μg/ml)
Recombinant DNA reagent	Amber-free HIV-1_{Q23} Env_{BG505} ΔRT WT	Addgene, Maolin Lu Lab, UT Tyler	Cat# 213007	
Recombinant DNA reagent	Amber-free HIV-1_{Q23} Env_{BG505} ΔRT $S401^{TAG}$ $R542^{TAG}$	This paper, Maolin Lu Lab, UT Tyler		This construct is available upon request made to the corresponding author
Recombinant DNA reagent	$tRNA^{Pyl}$/$NESPyIRS^{AF}$	Edward Lemke Lab, Johannes Gutenberg University Mainz		
Recombinant DNA reagent	HIV-1-InGluc	Maolin Lu Lab, UT Tyler		
Peptide, recombinant protein	Soluble CD4	Priyamvada Acharya Lab, Duke University		smFRET (100 μg/ml)
Chemical compound, drug	Polyethylenimine (PEI)	Polyscience	Cat# NC1014320	
Chemical compound, drug	Trans-cyclooct-2-en-L-lysine (TCO*A)	Sichem	Cat# SC8008	
Chemical compound, drug	LD555-TTZ	Lumidyne Technologies	Cat# 99	Custom synthesis
Chemical compound, drug	LD655-TTZ	Lumidyne Technologies	Cat# 99	Custom synthesis
Chemical compound, drug	Opti-prep	Sigma	Cat# D1556	
Chemical compound, drug	BCN-OH quencher	Sigma	Cat# 742678	
Chemical compound, drug	Protocatechuic acid (PCA)	Sigma	Cat# PHL89766	
Chemical compound, drug	Protocatechuate 3,4-dioxygenase (PCD)	Sigma	Cat# P8279	
Chemical compound, drug	Aldrithiol-2	Sigma	Cat# 143049	

Reagent type (species) or resource	Designation	Source or reference	Identifiers	Additional information
Chemical compound, drug	DSPE-PEG (2000) Biotin	Avanti Research	Cat# A88129	
Chemical compound, drug	Mycoplasma PCR detection kit	Millipore Sigma	Cat# MP0050-100TST	
Software, algorithm	MATLAB	MathWorks	RRID:SCR_001622	
Software, algorithm	GraphPad Prism 10	GraphPad	RRID:SCR_002798	
Software, algorithm	PyMOL	PyMOL	RRID:SCR_000305	

Cell lines and cell maintenance

We obtained all cell lines used in this study from ATCC or BEI resources. HEK293T cells (ATCC # CRL-3216) were used for producing replication-defective HIV-1 viruses. TZM-bl cells (BEI Resources # HRP-8129), which stably express the receptor CD4 and the co-receptor CCR5, were used as target cells to quantify the infectivity of the produced HIV-1 viruses and to assess the neutralizing activity of antibodies. These cell lines were cultured in high glucose Dulbecco's Modified Eagle Medium (Gibco # 11965-092) supplemented with 10% (vol/vol) heat-inactivated fetal bovine serum (Gemini Bio # 100-106), 100 mg/ml penicillin–streptomycin (Gibco # 15140-122), and 6 mM L-glutamine (Gibco # 25030-081), and maintained in a 37°C incubator supplied with 5% CO_2. In our laboratory, cell lines were verified by microscopic examination of cellular morphology and growth-curve analysis, and were routinely tested by PCR (Millipore Sigma # MP0050-100TST) to confirm that they were Mycoplasma-negative. Cells used for experiments were maintained between passages 3 and 10.

Plasmid construction

Tagged Env plasmids used in this study were constructed by site-directed mutagenesis using the Amber-free HIV-1_{Q23} Env_{BG505} ΔRT (Addgene # 213007; ***Ao et al., 2024***) plasmid as a template. The plasmid HIV-1_{Q23} Env_{BG505} carries the gene encoding the Env protein from the BG505 strain, while all non-Env HIV-1 genes are derived from the HIV-1 Q23 strain (***Poss and Overbaugh, 1999***; ***Haddox et al., 2018***). Plasmid HIV-1_{Q23} Env_{BG505} ΔRT was made by deleting the gene encoding the reverse transcriptase (RT) from the parental construct (***Ma et al., 2018***). The amber-free HIV-1_{Q23} Env_{BG505} ΔRT (Addgene # 213007) plasmid was created from HIV-1_{Q23} Env_{BG505} ΔRT by substituting all TAG (amber) stop codons in the Pol, Vif, Vpu, and Rev genes with TAA (ochre) stop codons (***Ao et al., 2024***). The plasmid amber-free HIV-1_{Q23} Env_{BG505} $S401^{TAG}$ $R542^{TAG}$ was generated by introducing TAG stop codons at the codons corresponding to Ser401 and Arg542 within the Env sequence. The dual-amber Env_{BG505} $S401^{TAG}$ $R542^{TAG}$ construct was generated using a similar mutagenesis approach. All plasmids were amplified in Stbl3 competent cells (Invitrogen, #C7373-03) and verified by DNA sequencing prior to use.

Virus production

The preparation of HIV-1_{Q23} Env_{BG505} viral particles has been previously described (***Ma et al., 2018***; ***Ao et al., 2024***; ***Lu et al., 2019a***). Briefly, healthy, exponentially growing, and mycoplasma-free HEK293T cells were used to produce viral particles. One day prior to transfection, HEK293T cells were seeded into culture plates to ensure that cell confluency exceeded 70% at the time of transfection. The growth medium was then replaced with Opti-MEM, and the transfection complex was prepared by mixing polyethylenimine (PEI; 1 mg/ml) with plasmid DNA (amber-free HIV-1_{Q23} Env_{BG505} or its derivatives) at a 3:1 (vol:wt) ratio of PEI to total plasmid. The mixture was incubated at room temperature for 15 min before being added to the cells. For packaging HIV-1 viral particles carrying dual-amber mutant Env (such as $N136^{TAG}$ $S401^{TAG}$ or $S401^{TAG}$ $R542^{TAG}$) (***Ao et al., 2024***), an additional plasmid, $tRNA^{Pyl}$/$NESPyIRS^{AF}$ (a gift from the Edward Lemke Lab) (***Sakin et al., 2017***; ***Nikić et al., 2016***), was co-transfected to enable incorporation of the noncanonical/unnatural amino acid (ncAA). This plasmid encodes an aminoacyl-tRNA synthetase (aaRS) that incorporates ncAA into its cognate tRNA and was included at a 3:1 ratio relative to the Env plasmid. The ncAA trans-cyclooct-2-en-L-lysine (TCO*A; SiChem #SC8008) was added to the culture medium at a final concentration of 250 μM. For the preparation of viral particles used in subsequent infectivity and neutralization assays,

an additional plasmid, HIV-1-inGluc, encoding the secreted Gaussia luciferase (Gluc) enzyme, was included in the transfection mixture. Four to six hours after transfection, the transfection medium was replaced with complete growth medium, and the cells were incubated for 40 hr. The culture supernatant containing viral particles was collected, filtered through a 0.45-μm membrane filter (PALL #4654), and concentrated by ultracentrifugation through a 15% (w:v) sucrose cushion in PBS at 25,000 rpm for 2 hr using an SW28 rotor (Beckman Coulter). The resulting viral pellets were resuspended in PBS for subsequent use.

Western blotting

Virus particle preparations or cell lysates were mixed with Laemmli SDS sample buffer (Thermo Scientific, #J61337-AD) and heated at 95°C for 15 min. The denatured protein samples were separated on a 4–12% Bis-Tris gradient gel by SDS-PAGE and subsequently transferred onto a PVDF membrane using the Trans-Blot Turbo system (Bio-Rad, #1704150). The membrane was blocked with 5% (wt:vol) non-fat milk (RPI, #M17200) in TBST buffer at room temperature for 1 hr, followed by incubation with the primary antibody against HIV-1 gp120 (BEI Resources, #ARP-288) diluted in 5% non-fat milk/TBST at 4°C overnight. After washing the membrane three times with TBST (10 min each), it was incubated with HRP-conjugated anti-sheep IgG secondary antibody (Proteintech, #SA00001-16) at room temperature for 1 hr. The membrane was washed again three times with TBST, and protein bands were visualized using a chemiluminescent HRP substrate (Millipore, #WBKLS0500). Signal detection and quantification were performed with the ChemiDoc Imaging System (Bio-Rad) using Image Lab software.

Production of soluble CD4 and antibodies

The following monoclonal antibodies and proteins were expressed in Expi293 cells by transient transfection of heavy-light chain plasmids, followed by protein A affinity column, size exclusion chromatography, and buffer exchange to 20 mM PBS pH 7.5, 0.002% wt/vol azide, and then flash-frozen for use. Overall, antibodies 17b, DH51.2_K3, 8ANC195, VRC34, VRC42, PGT151, 10E8.4, iMab, and 10E8.4/iMab were produced in the same way. sCD4 was also expressed transiently and purified as described previously (***Thakur et al., 2025***).

HIV-1 infectivity and antibody neutralization

Infectivity and neutralization assays were performed as previously described (***Ao et al., 2024***). One day before the assay, TZM-bl cells were seeded into 96-well culture plates. For virus neutralization assays, antibodies were serially diluted in basic DMEM and transferred to a new 96-well plate at 100 μl per well, with four replicates for each concentration. Subsequently, 50 μl of virus solution was added to each well, mixed thoroughly, and incubated at 37°C for 1 hr. For infectivity assays, no antibody was added, and the virus solution was applied directly to the cells. After incubation, the culture medium from the TZM-bl cells was removed and replaced with 50 μl per well of DMEM containing 20% FBS. The antibody–virus mixtures (or virus alone for infectivity assays) were then added to the cells and incubated for 48 hr at 37°C. Following incubation, the plates were gently mixed, and 50 μl of the supernatant from each well was transferred to a white microtiter plate. Luminescence was measured using a BioTek Synergy H1 microplate reader equipped with an automatic injector, following the manufacturer's instructions for the Gaussia Luciferase Glow Assay Kit (Thermo, #16161). Data analysis was performed using GraphPad Prism software.

Diameter measurement of HIV-1 viral particles

The diameter distribution of HIV-1 virions diluted in BBS buffer was measured by nanoparticle tracking analysis using a ZetaView X30 instrument (Particle Metrix). After sample loading, the instrument automatically recorded videos across three cycles and 11 positions to track particle motion and calculate their hydrodynamic diameter and concentration based on the Stokes–Einstein equation. Data acquisition and analysis were performed using ZetaView software (version 8.05.16 SP3).

Cryo-ET sample preparation and tomogram reconstruction

Virus particles for the cryo-ET imaging were produced using the plasmid carrying the RT gene. After the supernatant containing HIV-1 virions was collected and filtered, the aldrithiol-2 (AT-2, Sigma # 143049) was added at a final concentration of 0.5 M and incubated at 4°C with rotation for 12–18 hr to inactivate the HIV-1 virus. The viral particles are then purified by sucrose density gradient centrifugation. Viral particles were mixed with a 6 nm gold tracer (Aurion). 4 µl of the mixture was placed onto freshly glow-discharged 200 mesh Cu Quantifoil R 2/1 grids, blotted for 5 s and plunge frozen in liquid ethane by using Vitrobot Mark IV (FEI Co). Vitrobot was maintained at 4°C and 100% humidity during all these experiments. Frozen grids were imaged using a 200 kV Glacios Selectris X with a Falcon 4i direct electron detector. Tilt-series were collected using a dose-symmetric tilting scheme from –51° to +51° with a step size of 3°, and Tomography 5 software (Thermo Fisher Scientific) was employed at approximately 5 µm defocus. Tilt-series were collected at a magnification of ×63,000, corresponding to a pixel size of 2.01 Å per pixel. The total dose per tilt series was ~80e^{-}/Å^2 distributed over 35 stacks. Each stack contains approximately ten images. We used IMOD to facilitate data processing, which includes drift correction of dose-fractionated data and assembly of corrected sums into tilt series, automatic fiducial seed model generation, alignment, and contrast transfer function correction of tilt series (***Kremer et al., 1996***) and weighted back projection reconstruction of tilt series into tomograms using Tomo3 (***Agulleiro and Fernandez, 2015***).

Preparation and fluorescent labeling of virus Env for smFRET

Viral particles used for smFRET analysis were RT-deleted and prepared using a method similar to that described previously (***Ao et al., 2024***). S401* R542* virions refer to dual-color, fluorescently labeled particles generated by incorporating noncanonical amino acids (ncAAs) at amber (TAG) codons corresponding to S401 on gp120 and R542 on gp41 via amber suppression, followed by fluorophore conjugation through click chemistry. N136* R542* virions were generated analogously.

During transfection, plasmids encoding amber-free HIV-1_{Q23} Env_{BG505} ΔRT and those carrying dual-amber Env variants (S401^{TAG} R542^{TAG} or N136^{TAG} S401^{TAG}) were mixed at a calculated ratio (4:1) based on their relative amber suppression efficiencies (~20%) of S401^{ncAA} R542^{ncAA} or N136^{ncAA} S401^{ncAA} Env on virions. By assuming random assembly of Env trimers, the use of a very diluted Env ratio (untagged Env: tagged Env = ~20:1) will ensure that most virions carrying wild-type Env trimers, and among those virions carrying a single dual-ncAA gp120 within an otherwise wild-type Env background could be subsequently fluorescently labeled and identified using single-molecule imaging.

Virus pellets were resuspended in labeling buffer containing 50 mM HEPES, 10 mM $MgCl_2$, and 10 mM $CaCl_2$. Fluorescent labeling of Env by click chemistry was performed as previously described (***Xu et al., 2025***; ***Ao et al., 2024***). Briefly, amber-free virions containing click-reactive TCO*A residues were incubated in a reaction mixture containing 0.1 mM tetrazine-conjugated Cy3 derivative (LD555-TTZ, Lumidyne) and Cy5 derivative (LD655-TTZ, Lumidyne) fluorophores at room temperature for approximately 6 hr. The reaction was quenched by the addition of 1 mM BCN-OH followed by incubation for 10 min. Subsequently, PEG2000-biotin was added to a final concentration of 0.1 mg/ml, and the mixture was incubated for 30 min at room temperature with rotation. Excess dye and lipids were removed by ultracentrifugation through a 6–18% Optiprep gradient at 40,000 rpm for 1 hr. Of note, clickable dyes can be randomly coupled to two ncAA TCO*A in Env trimer on the virus. Unlabeled and multi-labeled virions can be easily identified based on the correlation between synchronized two-channel fluorescence signals (as described below). The fluorescently labeled virions were then stored at –80°C until use.

Excitation and emission spectra characterization of virions

Viral particles were produced from the dual-amber Env S401^{TAG} R542^{TAG} construct using the methods described above. The concentrated viral preparation was divided into three equal aliquots and subjected to fluorescent labeling with LD555-TTZ (single labeling), LD655-TTZ (single labeling), or LD555-TTZ/LD655-TTZ (dual labeling), following the established viral labeling protocol. Excess unreacted dye was removed by sucrose density gradient centrifugation (5%, 10%, 15%, 20%, and 40% layers), and the viral fraction collected from above the 40% sucrose layer was used for spectral analysis.

Fluorescence excitation and emission spectra were recorded using a Horiba FluoroMax spectrofluorometer (FluoroMax Plus-C-SP). Excitation spectra were acquired over the visible wavelength

ranges (450–650 nm for LD555-TTZ and 550–700 nm for LD655-TTZ) at fixed emission wavelengths of 569 and 669 nm, respectively. Emission spectra were recorded over the ranges (550–700 nm for LD555-TTZ and 650–800 nm for LD655-TTZ) for each sample upon excitation at 532 or 640 nm. The intensity was normalized to the maximum value in each spectrum for comparison. The resulting data were analyzed and plotted using GraphPad Prism software. No spectral shifts were observed between the free LD555 or LD655 dyes and their conjugated forms on HIV-1 viral particles.

smFRET data acquisition

All smFRET experiments of Env on intact HIV-1 virions were performed using a customized prism-based total internal reflection fluorescence (prism-TIRF) microscope, as previously described (***Lee et al., 2024***; ***Thakur et al., 2025***; ***Ao et al., 2024***). Fluorescently labeled HIV-1 virions were incubated in the absence or presence of 0.1 mg/ml ligands or antibodies in imaging buffer containing 50 mM Tris (pH 7.4), 50 mM NaCl, a triplet-state quencher cocktail, 2 mM protocatechuic acid, and 8 nM protocatechuate 3,4-dioxygenase at room temperature for 30 min prior to imaging. Ligand and antibody concentrations were approximately fivefold above their 95% inhibitory concentration (5x IC95). Fluorescently labeled HIV-1 virions were immobilized on a PEG-passivated, biotinylated quartz–coverslip imaging chamber coated with streptavidin. Based on the refractive index difference between quartz and the aqueous buffer, an evanescent field was generated by total internal reflection of a 532-nm single-wavelength laser (Ventus, Laser Quantum) directed onto a prism. The donor fluorophore labeled on Env was excited by this evanescent TIRF field, and the resulting fluorescence from both donor and acceptor fluorophores was collected through a water-immersion Nikon objective (60×, NA 1.27). Emission signals were then separated using a MultiCam LS image splitter (Cairn Research) equipped with a dichroic filter (Chroma) and directed through ET590/50 and ET690/50 emission filters (Chroma) corresponding to donor and acceptor channels, respectively. Fluorescence signals were recorded simultaneously using two synchronized sCMOS cameras (Hamamatsu ORCA-Flash4.0 V3) at a frame rate of 25 Hz for 80 s. Where indicated, virions were pre-incubated with the appropriate ligand or antibody for 30 min at room temperature before imaging.

smFRET data processing and analysis

Data were viewed, processed, and analyzed by a customized SPARTAN software package (***Juette et al., 2016***) and MATLAB-based scripts, as described previously by us and others (***Munro et al., 2014***; ***Alsahafi et al., 2019***; ***Ma et al., 2018***; ***Lee et al., 2024***; ***Thakur et al., 2025***; ***Ao et al., 2024***; ***Das et al., 2018***). Image stacks from smFRET recordings (2000 frames over 80 s) were extracted as individual fluorescence time trajectories (fluorescence traces) corresponding to donor and acceptor signals from labeled HIV-1 virions. At the single-molecule level, background fluorescence was estimated and subtracted based on the signal intensity at single-step photobleaching points. The FRET efficiency (FRET values or FRET in graphs) was calculated according to FRET = $I_A/(I_D + \gamma I_A)$, where I_D and I_A represent fluorescence intensities of the donor and acceptor, respectively, and the correlation coefficient γ compensates for crosstalk and differences in detection efficiency between two channels. The resulting FRET traces, time-resolved donor-to-acceptor energy transfer trajectories, reflect dynamic distance changes between the fluorophores, corresponding to real-time conformational dynamics of Env in the context of intact virions.

To ensure data quality, stringent filtering criteria were applied. Fluorescence traces were automatically excluded if signals from either donor or acceptor were missing, if multiple fluorophores were present, or if signal-to-noise ratios were insufficient. Remaining traces were manually viewed to confirm anti-correlation between donor and acceptor intensities, a hallmark of genuine FRET events reflecting conformational transitions of active Env molecules. Only traces exhibiting this anti-correlation and consistent single-protomer labeling were retained for further analysis.

Accepted FRET traces were compiled into FRET histograms (conformational ensembles), representing the distribution of Env conformational states across multiple virions. Each histogram represents the mean ± SEM, determined from three randomly assigned subsets of FRET traces under identical experimental conditions. The number of FRET states was inferred by combining visual inspection of FRET trajectories with iterative HMM (***McKinney et al., 2006***; ***Qin, 2004***). Model initialization was guided by visually identified transitions and optimized through iterative segmentation and semi-automatic parameter refinement. Statistical evaluation of model fits indicated that a three-state model

provided the simplest and most accurate representation of the data, yielding lower log-likelihood values than a two-state model and avoiding overfitting.

FRET histograms were further fitted to the sum of three Gaussian distributions using a least-squares fitting algorithm in MATLAB. Each Gaussian component represented a distinct conformational state of Env, and the area under each Gaussian estimated the relative occupancy of that state. Relative state occupancies are reported as mean ± SEM, derived from the fitted histograms. The corresponding fitting parameters are summarized in ***Supplementary file 1***. The three FRET states correspond to distinct and reproducible conformational populations under different experimental conditions, consistent with previous Env smFRET studies employing different probe positions (***Munro et al., 2014***; ***Ma et al., 2018***; ***Ao et al., 2024***; ***Lu, 2021***).

Transition rates were derived from the above-mentioned FRET trace idealization, in which each FRET trajectory was converted into a time-correlated sequence of discrete states using a segmental *K*-means algorithm within an HMM framework (***McKinney et al., 2006***; ***Qin, 2004***). State-to-state transitions, indicating the locations and frequencies of conformational changes, were visualized as TDPs. Dwell time distributions, representing the duration a molecule remains in a specific conformational state before transitioning to another, were compiled into survival probability plots and fitted to a bi-exponential decay function ($y = A_1 \exp^{-k1t} + A_2 \exp^{-k2t}$). A_1 and A_2 are the amplitudes, and $k1$ and $k2$ are the corresponding rate constants. The overall transition rate was determined as the amplitude-weighted average of the two rate constants.

Molecular dynamics simulation and analysis

Atomic coordinates of HIV-1 Env in the PC state were obtained by predicting the structure of the Env trimer using AlphaFold3. The input sequence consisted of three gp120 subunits (residues 30–505) and three gp41 subunits (residues 509–661) derived from HIV-1 BG505 Env (UniProt ID Q2N0S5). To enable site-specific fluorophore labeling, residues S398 in gp120 and R539 in gp41 of a single protomer were mutated to canonical lysine residues. The top-ranked predicted model showed acceptable agreement with the experimentally determined PC Env structure (RCSB PDB ID: 4TVP), (***Pancera et al., 2014***) with a backbone RMSD of 0.82 Å. Atomic coordinates of Env in the CO state were based on the experimentally solved structure (RCSB PDB ID: 5VN3) (***Ozorowski et al., 2017***). Residues R542 (chain A) and T401 (chain J) were mutated to lysine residues using PyMOL (Schrödinger).

Atomic coordinates for the two fluorophores and linkers were generated with MarvinSketch (Chemaxon) and PyMOL. Force-field parameters for the fluorophores were generated using a fragment-based parameterization strategy. The fluorophores alone and model compounds consisting of the fluorophore covalently linked to a lysine side-chain fragment were both parameterized using GAFF/GAFF2, with AM1-BCC partial charges assigned using Antechamber. The latter was used to capture the local electronic environment introduced by covalent conjugation. During construction of the full fluorophore–protein conjugates, atom types and partial charges associated with the covalent linkage were assigned by transferring consistent parameter trends from the fluorophore–lysine model compounds, while preserving the original fluorophore parameters wherever applicable. The fluorophores were assembled with the protein, and the assembly was visualized in VMD. Final system preparation, including definition of covalent linkages and generation of topology and coordinate files, was performed using LEaP in AmberTools.

Each system was neutralized and solvated in explicit TIP3P water with periodic boundary conditions. Sodium and chloride ions were added to achieve a final salt concentration of 150 mM NaCl. Protein atoms were described using the Amber ff14SB force field.

Energy minimization was performed in multiple stages, followed by gradual heating from 0 to 300 K under constant volume (NVT) conditions. The systems were subsequently equilibrated under constant pressure (NPT) conditions at 1 atm to stabilize system density.

Following equilibration, a pre-production simulation was carried out under NPT conditions for 200 ps with weak positional restraints applied to the protein backbone. Production simulations were then performed in the NPT ensemble at 300 K and 1 atm with all restraints removed. Atomic coordinates were saved every 5 ps. For each labeled system, three independent production trajectories of 10 ns were generated using different initial velocity seeds.

Dye positions sampled throughout the production trajectories were extracted for every simulation frame. All trajectory frames were structurally aligned to the protein backbone. The protein structure

from a reference frame was retained, while fluorophore coordinates from all frames were superimposed to generate a composite dye ensemble representation.

Inter-dye distances were calculated on a per-frame basis using the center-of-mass coordinates of the fluorophore chromophores. Distance time traces were obtained directly from the production trajectories and smoothed using a centered moving average with a time window of 0.4 ns.

Acknowledgements

The authors thank Yuanyun Ao for the valuable discussions and contributions during the early stages of this study. The following reagent was obtained through BEI Resources, NIAID, NIH: Monoclonal Anti-Human Immunodeficiency Virus Type 1 (HIV-1) gp120 (PG16), ARP-12150. Research reported in this publication was supported by the National Institute of Allergy and Infectious Diseases of the National Institutes of Health (NIH) under Award Number R01AI181600 to ML. The content is solely the responsibility of the authors and does not necessarily represent the official views of the NIH. This research was also supported in part by the Intramural Research Program of the NIH. The contributions of the NIH authors were made as part of their official duties as NIH federal employees, are in compliance with agency policy requirements, and are considered Works of the United States Government. However, the findings and conclusions presented in this paper are those of the authors and do not necessarily reflect the views of the NIH or the U.S. Department of Health and Human Services.

Additional information

Funding

Funder	Grant reference number	Author
National Institute of Allergy and Infectious Diseases	R01AI181600	Maolin Lu

The funders had no role in study design, data collection, and interpretation, or the decision to submit the work for publication.

Author contributions

Wang Xu, Data curation, Formal analysis, Investigation, Visualization, Writing – original draft; Narendra Kumar Gonepudi, Data curation, Formal analysis, Visualization; Junyu Liu, Data curation, Formal analysis, Validation, Methodology, Writing – review and editing; Yufan He, Data curation, Software, Visualization, Methodology; Revansiddha Katte, Data curation, Formal analysis; Ran Wang, Data curation, Visualization, Methodology; Harry Baffour Awuah, Data curation; Yang Han, Data curation, Project administration; Baoshan Zhang, Jian Yu, Resources; Bo Hu, Data curation, Supervision, Methodology; David D Ho, Resources, Supervision; Priyamvada Acharya, Peter D Kwong, Resources, Supervision, Writing – review and editing; Maolin Lu, Conceptualization, Software, Formal analysis, Supervision, Funding acquisition, Validation, Investigation, Methodology, Writing – original draft, Project administration, Writing – review and editing

Author ORCIDs

Wang Xu https://orcid.org/0000-0003-4452-9240
Priyamvada Acharya https://orcid.org/0000-0002-0089-277X
Peter D Kwong https://orcid.org/0000-0003-3560-232X
Maolin Lu https://orcid.org/0000-0002-8099-6447

Peer review material

Version of Record:
Reviewer #1 (Public review): https://doi.org/10.7554/eLife.110887.3.sa1
Reviewer #2 (Public review): https://doi.org/10.7554/eLife.110887.3.sa2
Author response https://doi.org/10.7554/eLife.110887.3.sa3

Reviewed preprint v2
Reviewer #1 (Public review): https://doi.org/10.7554/eLife.110887.2.sa2

Reviewer #2 (Public review): https://doi.org/10.7554/eLife.110887.2.sa1
Author response: https://doi.org/10.7554/eLife.110887.2.sa0
eLife Assessment https://doi.org/10.7554/eLife.110887.2.sa3

Reviewed preprint v1
Reviewer #1 (Public review): https://doi.org/10.7554/eLife.110887.1.sa2
Reviewer #2 (Public review): https://doi.org/10.7554/eLife.110887.1.sa1
Author response: https://doi.org/10.7554/eLife.110887.1.sa0
eLife Assessment https://doi.org/10.7554/eLife.110887.1.sa3

Additional files

Supplementary files

Supplementary file 1. Model-fitting statistics and parameters for FRET histograms.

Supplementary file 2. Amino acid sequences of heavy and light chains of antibodies used in this study.

MDAR checklist

Data availability

Data supporting the findings of this study are available within the paper and its supplementary files. We have provided source data files containing the numerical data used to generate the figures.

References

Agulleiro JI, Fernandez JJ. 2015. Tomo3D 2.0--exploitation of advanced vector extensions (AVX) for 3D reconstruction. *Journal of Structural Biology* **189**:147–152. DOI: https://doi.org/10.1016/j.jsb.2014.11.009, PMID: 25528570

Alsahafi N, Bakouche N, Kazemi M, Richard J, Ding S, Bhattacharyya S, Das D, Anand SP, Prévost J, Tolbert WD, Lu H, Medjahed H, Gendron-Lepage G, Ortega Delgado GG, Kirk S, Melillo B, Mothes W, Sodroski J, Smith AB, Kaufmann DE, et al. 2019. An asymmetric opening of HIV-1 envelope mediates antibody-dependent cellular cytotoxicity. *Cell Host & Microbe* **25**:578–587. DOI: https://doi.org/10.1016/j.chom.2019.03.002, PMID: 30974085

Ao Y, Grover JR, Gifford L, Han Y, Zhong G, Katte R, Li W, Bhattacharjee R, Zhang B, Sauve S, Qin W, Ghimire D, Haque MA, Arthos J, Moradi M, Mothes W, Lemke EA, Kwong PD, Melikyan GB, Lu M. 2024. Bioorthogonal click labeling of an amber-free HIV-1 provirus for in-virus single molecule imaging. *Cell Chemical Biology* **31**:487–501. DOI: https://doi.org/10.1016/j.chembiol.2023.12.017, PMID: 38232732

Banach BB, Pletnev S, Olia AS, Xu K, Zhang B, Rawi R, Bylund T, Doria-Rose NA, Nguyen TD, Fahad AS, Lee M, Lin BC, Liu T, Louder MK, Madan B, McKee K, O'Dell S, Sastry M, Schön A, Bui N, et al. 2023. Antibody-directed evolution reveals a mechanism for enhanced neutralization at the HIV-1 fusion peptide site. *Nature Communications* **14**:7593. DOI: https://doi.org/10.1038/s41467-023-42098-5, PMID: 37989731

Bennett AL, Henderson R. 2021. HIV-1 envelope conformation, allostery, and dynamics. *Viruses* **13**:852. DOI: https://doi.org/10.3390/v13050852, PMID: 34067073

Blackman ML, Royzen M, Fox JM. 2008. Tetrazine ligation: fast bioconjugation based on inverse-electron-demand Diels-Alder reactivity. *Journal of the American Chemical Society* **130**:13518–13519. DOI: https://doi.org/10.1021/ja8053805, PMID: 18798613

Blattner C, Lee JH, Sliepen K, Derking R, Falkowska E, de la Peña AT, Cupo A, Julien JP, van Gils M, Lee PS, Peng W, Paulson JC, Poignard P, Burton DR, Moore JP, Sanders RW, Wilson IA, Ward AB. 2014. Structural delineation of a quaternary, cleavage-dependent epitope at the gp41-gp120 interface on intact HIV-1 Env trimers. *Immunity* **40**:669–680. DOI: https://doi.org/10.1016/j.immuni.2014.04.008, PMID: 24768348

Brandenberg OF, Magnus C, Regoes RR, Trkola A. 2015a. The HIV-1 entry process: a stoichiometric view. *Trends in Microbiology* **23**:763–774. DOI: https://doi.org/10.1016/j.tim.2015.09.003, PMID: 26541228

Brandenberg OF, Magnus C, Rusert P, Regoes RR, Trkola A. 2015b. Different infectivity of HIV-1 strains is linked to number of envelope trimers required for entry. *PLOS Pathogens* **11**:e1004595. DOI: https://doi.org/10.1371/journal.ppat.1004595, PMID: 25569556

Buzon V, Natrajan G, Schibli D, Campelo F, Kozlov MM, Weissenhorn W. 2010. Crystal structure of HIV-1 gp41 including both fusion peptide and membrane proximal external regions. *PLOS Pathogens* **6**:e1000880. DOI: https://doi.org/10.1371/journal.ppat.1000880, PMID: 20463810

Chatterjee D, Niu L, Medjahed H, Ding S, Benlarbi M, Bélanger É, Prévost J, Chen HC, Tolbert WD, Smith AB, Pazgier M, Finzi A. 2025. A gp41 HR2 residue modulates the susceptibility of HIV-1 envelope glycoproteins to small molecule inhibitors targeting gp120. *Journal of Virology* **99**:e0226724. DOI: https://doi.org/10.1128/jvi.02267-24, PMID: 40145736

Chen B. 2019. Molecular mechanism of HIV-1 entry. *Trends in Microbiology* **27**:878–891. DOI: https://doi.org/10.1016/j.tim.2019.06.002, PMID: 31262533

Croft JT, Do HN, Leaman DP, Lovendahl KN, Ralli-Jain P, Chase KJ, Chen C, Prasad VM, Derdeyn CA, Zwick MB, Gnanakaran S, Lee KK. 2026. Structure of HIV-1 Env Glycoprotein on Virions Reveals an Alternative Fusion Subunit Organization and Native Membrane Coupling. *bioRxiv*. DOI: https://doi.org/10.64898/2026.01.09.698652, PMID: 41542432

Dam KMA, Fan C, Yang Z, Bjorkman PJ. 2023. Intermediate conformations of CD4-bound HIV-1 Env heterotrimers. *Nature* **623**:1017–1025. DOI: https://doi.org/10.1038/s41586-023-06639-8, PMID: 37993719

Das DK, Govindan R, Nikić-Spiegel I, Krammer F, Lemke EA, Munro JB. 2018. Direct visualization of the conformational dynamics of single influenza hemagglutinin trimers. *Cell* **174**:926–937. DOI: https://doi.org/10.1016/j.cell.2018.05.050, PMID: 29961575

Das DK, Bulow U, Diehl WE, Durham ND, Senjobe F, Chandran K, Luban J, Munro JB. 2020. Conformational changes in the Ebola virus membrane fusion machine induced by pH, Ca2+, and receptor binding. *PLOS Biology* **18**:e3000626. DOI: https://doi.org/10.1371/journal.pbio.3000626, PMID: 32040508

Flemming J, Wiesen L, Herschhorn A. 2018. Conformation-dependent interactions between HIV-1 envelope glycoproteins and broadly neutralizing antibodies. *AIDS Research and Human Retroviruses* **34**:794–803. DOI: https://doi.org/10.1089/AID.2018.0102, PMID: 29905080

Foulkes C, Friedrich N, Ivan B, Stiegeler E, Magnus C, Schmidt D, Karakus U, Weber J, Günthard HF, Pasin C, Rusert P, Trkola A. 2025. Assessing bnAb potency in the context of HIV-1 envelope conformational plasticity. *PLOS Pathogens* **21**:e1012825. DOI: https://doi.org/10.1371/journal.ppat.1012825, PMID: 39836706

Gonepudi NK, Xu W, Awuah HB, Lu M. 2026. Bioorthogonal click-chemistry labeling and visualization of dual noncanonical amino acid-incorporated HIV-1 Env on intact virions. *Methods in Enzymology* **731**:167–191. DOI: https://doi.org/10.1016/bs.mie.2026.05.005, PMID: 42349954

Haddox HK, Dingens AS, Hilton SK, Overbaugh J, Bloom JD. 2018. Mapping mutational effects along the evolutionary landscape of HIV envelope. *eLife* **7**:e34420. DOI: https://doi.org/10.7554/eLife.34420, PMID: 29590010

Haynes BF, Burton DR, Mascola JR. 2019. Multiple roles for HIV broadly neutralizing antibodies. *Science Translational Medicine* **11**:eaaz2686. DOI: https://doi.org/10.1126/scitranslmed.aaz2686, PMID: 31666399

Haynes BF, Wiehe K, Borrow P, Saunders KO, Korber B, Wagh K, McMichael AJ, Kelsoe G, Hahn BH, Alt F, Shaw GM. 2023. Strategies for HIV-1 vaccines that induce broadly neutralizing antibodies. *Nature Reviews. Immunology* **23**:142–158. DOI: https://doi.org/10.1038/s41577-022-00753-w, PMID: 35962033

Henderson R, Lu M, Zhou Y, Mu Z, Parks R, Han Q, Hsu AL, Carter E, Blanchard SC, Edwards RJ, Wiehe K, Saunders KO, Borgnia MJ, Bartesaghi A, Mothes W, Haynes BF, Acharya P, Munir Alam S. 2020. Disruption of the HIV-1 Envelope allosteric network blocks CD4-induced rearrangements. *Nature Communications* **11**:520. DOI: https://doi.org/10.1038/s41467-019-14196-w, PMID: 31980614

Herschhorn A, Ma X, Gu C, Ventura JD, Castillo-Menendez L, Melillo B, Terry DS, Smith AB III, Blanchard SC, Munro JB, Mothes W, Finzi A, Sodroski J. 2016. Release of gp120 restraints leads to an entry-competent intermediate state of the HIV-1 envelope glycoproteins. *mBio* **7**:e01598. DOI: https://doi.org/10.1128/mBio.01598-16, PMID: 27795397

Herschhorn A, Gu C, Moraca F, Ma X, Farrell M, Smith AB, Pancera M, Kwong PD, Schön A, Freire E, Abrams C, Blanchard SC, Mothes W, Sodroski JG. 2017. The β20-β21 of gp120 is a regulatory switch for HIV-1 Env conformational transitions. *Nature Communications* **8**:1049. DOI: https://doi.org/10.1038/s41467-017-01119-w, PMID: 29051495

Huang J, Ofek G, Laub L, Louder MK, Doria-Rose NA, Longo NS, Imamichi H, Bailer RT, Chakrabarti B, Sharma SK, Alam SM, Wang T, Yang Y, Zhang B, Migueles SA, Wyatt R, Haynes BF, Kwong PD, Mascola JR, Connors M. 2012. Broad and potent neutralization of HIV-1 by a gp41-specific human antibody. *Nature* **491**:406–412. DOI: https://doi.org/10.1038/nature11544, PMID: 23151583

Huang Y, Yu J, Lanzi A, Yao X, Andrews CD, Tsai L, Gajjar MR, Sun M, Seaman MS, Padte NN, Ho DD. 2016. Engineered bispecific antibodies with exquisite HIV-1-neutralizing activity. *Cell* **165**:1621–1631. DOI: https://doi.org/10.1016/j.cell.2016.05.024, PMID: 27315479

Ivan B, Sun Z, Subbaraman H, Friedrich N, Trkola A. 2019. CD4 occupancy triggers sequential pre-fusion conformational states of the HIV-1 envelope trimer with relevance for broadly neutralizing antibody activity. *PLOS Biology* **17**:e3000114. DOI: https://doi.org/10.1371/journal.pbio.3000114, PMID: 30650070

Juette MF, Terry DS, Wasserman MR, Altman RB, Zhou Z, Zhao H, Blanchard SC. 2016. Single-molecule imaging of non-equilibrium molecular ensembles on the millisecond timescale. *Nature Methods* **13**:341–344. DOI: https://doi.org/10.1038/nmeth.3769, PMID: 26878382

Katte RH, Xu W, Han Y, Hong X, Lu M. 2025. Inter-protomer opening cooperativity of envelope trimers positively correlates with HIV-1 entry stoichiometry. *mBio* **16**:e0275424. DOI: https://doi.org/10.1128/mbio.02754-24, PMID: 39998217

Klasse PJ. 2007. Modeling how many envelope glycoprotein trimers per virion participate in human immunodeficiency virus infectivity and its neutralization by antibody. *Virology* **369**:245–262. DOI: https://doi.org/10.1016/j.virol.2007.06.044, PMID: 17825343

Klasse PJ, Sanders RW, Ward AB, Wilson IA, Moore JP. 2025. The HIV-1 envelope glycoprotein: structure, function and interactions with neutralizing antibodies. *Nature Reviews. Microbiology* **23**:734–752. DOI: https://doi.org/10.1038/s41579-025-01206-6, PMID: 40702326

Kong R, Xu K, Zhou T, Acharya P, Lemmin T, Liu K, Ozorowski G, Soto C, Taft JD, Bailer RT, Cale EM, Chen L, Choi CW, Chuang G-Y, Doria-Rose NA, Druz A, Georgiev IS, Gorman J, Huang J, Joyce MG, et al. 2016. Fusion

peptide of HIV-1 as a site of vulnerability to neutralizing antibody. *Science* **352**:828–833. DOI: https://doi.org/10.1126/science.aae0474, PMID: 27174988

Krebs SJ, Kwon YD, Schramm CA, Law WH, Donofrio G, Zhou KH, Gift S, Dussupt V, Georgiev IS, Schätzle S, McDaniel JR, Lai Y-T, Sastry M, Zhang B, Jarosinski MC, Ransier A, Chenine AL, Asokan M, Bailer RT, Bose M, et al. 2019. Longitudinal analysis reveals early development of three MPER-directed neutralizing antibody lineages from an HIV-1-infected individual. *Immunity* **50**:677–691. DOI: https://doi.org/10.1016/j.immuni.2019.02.008, PMID: 30876875

Kremer JR, Mastronarde DN, McIntosh JR. 1996. Computer visualization of three-dimensional image data using IMOD. *Journal of Structural Biology* **116**:71–76. DOI: https://doi.org/10.1006/jsbi.1996.0013, PMID: 8742726

Kwon YD, Pancera M, Acharya P, Georgiev IS, Crooks ET, Gorman J, Joyce MG, Guttman M, Ma X, Narpala S, Soto C, Terry DS, Yang Y, Zhou T, Ahlsen G, Bailer RT, Chambers M, Chuang G-Y, Doria-Rose NA, Druz A, et al. 2015. Crystal structure, conformational fixation and entry-related interactions of mature ligand-free HIV-1 Env. *Nature Structural & Molecular Biology* **22**:522–531. DOI: https://doi.org/10.1038/nsmb.3051, PMID: 26098315

Kwon YD, Georgiev IS, Ofek G, Zhang B, Asokan M, Bailer RT, Bao A, Caruso W, Chen X, Choe M, Druz A, Ko S-Y, Louder MK, McKee K, O'Dell S, Pegu A, Rudicell RS, Shi W, Wang K, Yang Y, et al. 2016. Optimization of the solubility of HIV-1-neutralizing antibody 10e8 through somatic variation and structure-based design. *Journal of Virology* **90**:5899–5914. DOI: https://doi.org/10.1128/JVI.03246-15, PMID: 27053554

Kwong PD, Wyatt R, Robinson J, Sweet RW, Sodroski J, Hendrickson WA. 1998. Structure of an HIV gp120 envelope glycoprotein in complex with the CD4 receptor and a neutralizing human antibody. *Nature* **393**:648–659. DOI: https://doi.org/10.1038/31405, PMID: 9641677

Kwong PD, Doyle ML, Casper DJ, Cicala C, Leavitt SA, Majeed S, Steenbeke TD, Venturi M, Chaiken I, Fung M, Katinger H, Parren P, Robinson J, Van Ryk D, Wang L, Burton DR, Freire E, Wyatt R, Sodroski J, Hendrickson WA, et al. 2002. HIV-1 evades antibody-mediated neutralization through conformational masking of receptor-binding sites. *Nature* **420**:678–682. DOI: https://doi.org/10.1038/nature01188, PMID: 12478295

Kwong PD, Mascola JR. 2018. HIV-1 vaccines based on antibody identification, B cell ontogeny, and epitope structure. *Immunity* **48**:855–871. DOI: https://doi.org/10.1016/j.immuni.2018.04.029, PMID: 29768174

Ladinsky MS, Gnanapragasam PN, Yang Z, West AP, Kay MS, Bjorkman PJ. 2020. Electron tomography visualization of HIV-1 fusion with target cells using fusion inhibitors to trap the pre-hairpin intermediate. *eLife* **9**:e58411. DOI: https://doi.org/10.7554/eLife.58411, PMID: 32697193

Lee M, Lu M, Zhang B, Zhou T, Katte R, Han Y, Rawi R, Kwong PD. 2024. HIV-1-envelope trimer transitions from prefusion-closed to CD4-bound-open conformations through an occluded-intermediate state. *Computational and Structural Biotechnology Journal* **23**:4192–4204. DOI: https://doi.org/10.1016/j.csbj.2024.11.020, PMID: 39640534

Leonhardt SA, Purdy MD, Grover JR, Yang Z, Poulos S, McIntire WE, Tatham EA, Erramilli SK, Nosol K, Lai KK, Ding S, Lu M, Uchil PD, Finzi A, Rein A, Kossiakoff AA, Mothes W, Yeager M. 2023. Antiviral HIV-1 SERINC restriction factors disrupt virus membrane asymmetry. *Nature Communications* **14**:4368. DOI: https://doi.org/10.1038/s41467-023-39262-2, PMID: 37474505

Lerner E, Cordes T, Ingargiola A, Alhadid Y, Chung S, Michalet X, Weiss S. 2018. Toward dynamic structural biology: Two decades of single-molecule Förster resonance energy transfer. *Science* **359**:eaan1133. DOI: https://doi.org/10.1126/science.aan1133, PMID: 29348210

Li Z, Li W, Lu M, Bess J, Chao CW, Gorman J, Terry DS, Zhang B, Zhou T, Blanchard SC, Kwong PD, Lifson JD, Mothes W, Liu J. 2020. Subnanometer structures of HIV-1 envelope trimers on aldrithiol-2-inactivated virus particles. *Nature Structural & Molecular Biology* **27**:726–734. DOI: https://doi.org/10.1038/s41594-020-0452-2

Li W, Qin Z, Nand E, Grunst MW, Grover JR, Bess JW, Lifson JD, Zwick MB, Tagare HD, Uchil PD, Mothes W. 2023. HIV-1 Env trimers asymmetrically engage CD4 receptors in membranes. *Nature* **623**:1026–1033. DOI: https://doi.org/10.1038/s41586-023-06762-6, PMID: 37993716

Liu J, Bartesaghi A, Borgnia MJ, Sapiro G, Subramaniam S. 2008. Molecular architecture of native HIV-1 gp120 trimers. *Nature* **455**:109–113. DOI: https://doi.org/10.1038/nature07159, PMID: 18668044

Lu M, Ma X, Castillo-Menendez LR, Gorman J, Alsahafi N, Ermel U, Terry DS, Chambers M, Peng D, Zhang B, Zhou T, Reichard N, Wang K, Grover JR, Carman BP, Gardner MR, Nikić-Spiegel I, Sugawara A, Arthos J, Lemke EA, et al. 2019a. Associating HIV-1 envelope glycoprotein structures with states on the virus observed by smFRET. *Nature* **568**:415–419. DOI: https://doi.org/10.1038/s41586-019-1101-y, PMID: 30971821

Lu M, Ma X, Mothes W. 2019b. Illuminating the virus life cycle with single-molecule FRET imaging. *Advances in Virus Research* **105**:239–273. DOI: https://doi.org/10.1016/bs.aivir.2019.07.004, PMID: 31522706

Lu M, Uchil PD, Li W, Zheng D, Terry DS, Gorman J, Shi W, Zhang B, Zhou T, Ding S, Gasser R, Prévost J, Beaudoin-Bussières G, Anand SP, Laumaea A, Grover JR, Liu L, Ho DD, Mascola JR, Finzi A, et al. 2020. Real-time conformational dynamics of SARS-CoV-2 spikes on virus particles. *Cell Host & Microbe* **28**:880–891. DOI: https://doi.org/10.1016/j.chom.2020.11.001

Lu M. 2021. Single-molecule FRET imaging of virus spike-host interactions. *Viruses* **13**:332. DOI: https://doi.org/10.3390/v13020332, PMID: 33669922

Lyumkis D, Julien JP, de Val N, Cupo A, Potter CS, Klasse PJ, Burton DR, Sanders RW, Moore JP, Carragher B, Wilson IA, Ward AB. 2013. Cryo-EM structure of a fully glycosylated soluble cleaved HIV-1 envelope trimer. *Science* **342**:1484–1490. DOI: https://doi.org/10.1126/science.1245627, PMID: 24179160

Ma X, Lu M, Gorman J, Terry DS, Hong X, Zhou Z, Zhao H, Altman RB, Arthos J, Blanchard SC, Kwong PD, Munro JB, Mothes W. 2018. HIV-1 Env trimer opens through an asymmetric intermediate in which individual protomers adopt distinct conformations. *eLife* **7**:e34271. DOI: https://doi.org/10.7554/eLife.34271, PMID: 29561264

McKinney SA, Joo C, Ha T. 2006. Analysis of single-molecule FRET trajectories using hidden Markov modeling. *Biophysical Journal* **91**:1941–1951. DOI: https://doi.org/10.1529/biophysj.106.082487, PMID: 16766620

Munro JB, Gorman J, Ma X, Zhou Z, Arthos J, Burton DR, Koff WC, Courter JR, Smith AB, Kwong PD, Blanchard SC, Mothes W. 2014. Conformational dynamics of single HIV-1 envelope trimers on the surface of native virions. *Science* **346**:759–763. DOI: https://doi.org/10.1126/science.1254426, PMID: 25298114

Munro JB, Mothes W. 2015. Structure and dynamics of the native HIV-1 Env trimer. *Journal of Virology* **89**:5752–5755. DOI: https://doi.org/10.1128/JVI.03187-14, PMID: 25762739

Nikić I, Kang JH, Girona GE, Aramburu IV, Lemke EA. 2015. Labeling proteins on live mammalian cells using click chemistry. *Nature Protocols* **10**:780–791. DOI: https://doi.org/10.1038/nprot.2015.045, PMID: 25906116

Nikić I, Lemke EA. 2015. Genetic code expansion enabled site-specific dual-color protein labeling: superresolution microscopy and beyond. *Current Opinion in Chemical Biology* **28**:164–173. DOI: https://doi.org/10.1016/j.cbpa.2015.07.021, PMID: 26302384

Nikić I, Estrada Girona G, Kang JH, Paci G, Mikhaleva S, Koehler C, Shymanska NV, Ventura Santos C, Spitz D, Lemke EA. 2016. Debugging eukaryotic genetic code expansion for site-specific click-PAINT super-resolution microscopy. *Angewandte Chemie* **55**:16172–16176. DOI: https://doi.org/10.1002/anie.201608284, PMID: 27804198

Ozorowski G, Pallesen J, de Val N, Lyumkis D, Cottrell CA, Torres JL, Copps J, Stanfield RL, Cupo A, Pugach P, Moore JP, Wilson IA, Ward AB. 2017. Open and closed structures reveal allostery and pliability in the HIV-1 envelope spike. *Nature* **547**:360–363. DOI: https://doi.org/10.1038/nature23010, PMID: 28700571

Padte NN, Yu J, Huang Y, Ho DD. 2018. Engineering multi-specific antibodies against HIV-1. *Retrovirology* **15**:60. DOI: https://doi.org/10.1186/s12977-018-0439-9, PMID: 30157871

Pancera M, Zhou T, Druz A, Georgiev IS, Soto C, Gorman J, Huang J, Acharya P, Chuang GY, Ofek G, Stewart-Jones GBE, Stuckey J, Bailer RT, Joyce MG, Louder MK, Tumba N, Yang Y, Zhang B, Cohen MS, Haynes BF, et al. 2014. Structure and immune recognition of trimeric pre-fusion HIV-1 Env. *Nature* **514**:455–461. DOI: https://doi.org/10.1038/nature13808, PMID: 25296255

Parthasarathy D, Pothula KR, Ratnapriya S, Cervera Benet H, Parsons R, Huang X, Sammour S, Janowska K, Harris M, Sodroski J, Acharya P, Herschhorn A. 2024. Conformational flexibility of HIV-1 envelope glycoproteins modulates transmitted/founder sensitivity to broadly neutralizing antibodies. *Nature Communications* **15**:7334. DOI: https://doi.org/10.1038/s41467-024-51656-4, PMID: 39187497

Plass T, Milles S, Koehler C, Schultz C, Lemke EA. 2011. Genetically encoded copper-free click chemistry. *Angewandte Chemie* **50**:3878–3881. DOI: https://doi.org/10.1002/anie.201008178, PMID: 21433234

Plass T, Milles S, Koehler C, Szymański J, Mueller R, Wiessler M, Schultz C, Lemke EA. 2012. Amino acids for Diels-Alder reactions in living cells. *Angewandte Chemie* **51**:4166–4170. DOI: https://doi.org/10.1002/anie.201108231, PMID: 22473599

Poss M, Overbaugh J. 1999. Variants from the diverse virus population identified at seroconversion of a clade A human immunodeficiency virus type 1-infected woman have distinct biological properties. *Journal of Virology* **73**:5255–5264. DOI: https://doi.org/10.1128/JVI.73.7.5255-5264.1999, PMID: 10364271

Qin F. 2004. Restoration of single-channel currents using the segmental k-means method based on hidden Markov modeling. *Biophysical Journal* **86**:1488–1501. DOI: https://doi.org/10.1016/S0006-3495(04)74217-4, PMID: 14990476

Richard J, Grunst MW, Niu L, Díaz-Salinas MA, Zhu L, Tolbert WD, Marchitto L, Zhou F, Bourassa C, Kim H, Boodapati SLT, Yang D, Chiu TJ, Chen HC, Benlarbi M, Beaudoin-Bussières G, Gottumukkala S, Li W, Dionne K, Bélanger É, et al. 2025. The asymmetric opening of HIV-1 Env by a potent CD4 mimetic enables anti-coreceptor binding site antibodies to mediate ADCC. *Nature Communications* **16**:10419. DOI: https://doi.org/10.1038/s41467-025-65866-x, PMID: 41326374

Roy R, Hohng S, Ha T. 2008. A practical guide to single-molecule FRET. *Nature Methods* **5**:507–516. DOI: https://doi.org/10.1038/nmeth.1208, PMID: 18511918

Ruprecht CR, Krarup A, Reynell L, Mann AM, Brandenberg OF, Berlinger L, Abela IA, Regoes RR, Günthard HF, Rusert P, Trkola A. 2011. MPER-specific antibodies induce gp120 shedding and irreversibly neutralize HIV-1. *The Journal of Experimental Medicine* **208**:439–454. DOI: https://doi.org/10.1084/jem.20101907, PMID: 21357743

Sakin V, Hanne J, Dunder J, Anders-Össwein M, Laketa V, Nikić I, Kräusslich H-G, Lemke EA, Müller B. 2017. A versatile tool for live-cell imaging and super-resolution nanoscopy studies of HIV-1 env distribution and mobility. *Cell Chemical Biology* **24**:635–645. DOI: https://doi.org/10.1016/j.chembiol.2017.04.007, PMID: 28457706

Scharf L, Scheid JF, Lee JH, West AP Jr, Chen C, Gao H, Gnanapragasam PNP, Mares R, Seaman MS, Ward AB, Nussenzweig MC, Bjorkman PJ. 2014. Antibody 8ANC195 reveals a site of broad vulnerability on the HIV-1 envelope spike. *Cell Reports* **7**:785–795. DOI: https://doi.org/10.1016/j.celrep.2014.04.001, PMID: 24767986

Shaik MM, Peng H, Lu J, Rits-Volloch S, Xu C, Liao M, Chen B. 2019. Structural basis of coreceptor recognition by HIV-1 envelope spike. *Nature* **565**:318–323. DOI: https://doi.org/10.1038/s41586-018-0804-9, PMID: 30542158

Sok D, Burton DR. 2018. Recent progress in broadly neutralizing antibodies to HIV. *Nature Immunology* **19**:1179–1188. DOI: https://doi.org/10.1038/s41590-018-0235-7, PMID: 30333615

Sougrat R, Bartesaghi A, Lifson JD, Bennett AE, Bess JW, Zabransky DJ, Subramaniam S. 2007. Electron tomography of the contact between T cells and SIV/HIV-1: implications for viral entry. *PLOS Pathogens* **3**:e63. DOI: https://doi.org/10.1371/journal.ppat.0030063, PMID: 17480119

Thakur B, Katte RH, Xu W, Janowska K, Sammour S, Henderson R, Lu M, Kwong PD, Acharya P. 2025. Conformational trajectory of the HIV-1 fusion peptide during CD4-induced envelope opening. *Nature Communications* **16**:4595. DOI: https://doi.org/10.1038/s41467-025-59721-2, PMID: 40382314

Walker LM, Phogat SK, Chan-Hui PY, Wagner D, Phung P, Goss JL, Wrin T, Simek MD, Fling S, Mitcham JL, Lehrman JK, Priddy FH, Olsen OA, Frey SM, Hammond PW, Kaminsky S, Zamb T, Moyle M, Koff WC, Poignard P, et al. 2009. Broad and potent neutralizing antibodies from an African donor reveal a new HIV-1 vaccine target. *Science* **326**:285–289. DOI: https://doi.org/10.1126/science.1178746, PMID: 19729618

Wang Q, Finzi A, Sodroski J. 2020. The conformational states of the HIV-1 envelope glycoproteins. *Trends in Microbiology* **28**:655–667. DOI: https://doi.org/10.1016/j.tim.2020.03.007, PMID: 32418859

Williams LD, Ofek G, Schätzle S, McDaniel JR, Lu X, Nicely NI, Wu L, Lougheed CS, Bradley T, Louder MK, McKee K, Bailer RT, O'Dell S, Georgiev IS, Seaman MS, Parks RJ, Marshall DJ, Anasti K, Yang G, Nie X, et al. 2017. Potent and broad HIV-neutralizing antibodies in memory B cells and plasma. *Science Immunology* **2**:eaal2200. DOI: https://doi.org/10.1126/sciimmunol.aal2200, PMID: 28783671

Wyatt R, Sodroski J. 1998. The HIV-1 envelope glycoproteins: fusogens, antigens, and immunogens. *Science* **280**:1884–1888. DOI: https://doi.org/10.1126/science.280.5371.1884, PMID: 9632381

Xu W, Gonepudi NK, Lu M. 2025. Protocol for click labeling of HIV-1 envelope on amber-free virions prepared using genetic code expansion. *STAR Protocols* **6**:103995. DOI: https://doi.org/10.1016/j.xpro.2025.103995, PMID: 40716060

Xu W, Gonepudi NK, Han Y, Lu M. 2026. Genetic code expansion for single noncanonical amino acid incorporation into SARS-CoV-2 Omicron spike on amber-free lentiviral particles. *Methods in Enzymology* **731**:141–165. DOI: https://doi.org/10.1016/bs.mie.2026.05.022, PMID: 42349953

Yang X, Kurteva S, Ren X, Lee S, Sodroski J. 2005. Stoichiometry of envelope glycoprotein trimers in the entry of human immunodeficiency virus type 1. *Journal of Virology* **79**:12132–12147. DOI: https://doi.org/10.1128/JVI.79.19.12132-12147.2005, PMID: 16160141

Yang X, Kurteva S, Ren X, Lee S, Sodroski J. 2006. Subunit stoichiometry of human immunodeficiency virus type 1 envelope glycoprotein trimers during virus entry into host cells. *Journal of Virology* **80**:4388–4395. DOI: https://doi.org/10.1128/JVI.80.9.4388-4395.2006, PMID: 16611898

Zhao C, Li H, Swartz TH, Chen BK. 2022. The HIV env glycoprotein conformational states on cells and viruses. *mBio* **13**:e0182521. DOI: https://doi.org/10.1128/mbio.01825-21, PMID: 35323042